Lithos 356–357 (2020) 105372

Contents lists available at ScienceDirect

Lithos

journal homepage: www.elsevier.com/locate/lithos

Research Article

Ordovician shoshonitic to ultrapotassic volcanism in the central Norwegian Caledonides: The result of sediment subduction, mantle metasomatism and mantle partial melting

B.H. Dalslåen [a,*], D. Gasser [b,c], T. Grenne [c], L.E. Augland [d], F. Corfu [a]

[a] Department of Geosciences, University of Oslo, Oslo, Norway
[b] Department of Environmental Sciences, Western Norway University of Applied Sciences, Sogndal, Norway
[c] Geological Survey of Norway, Trondheim, Norway
[d] CEED, University of Oslo, Norway

ARTICLE INFO

Article history:
Received 23 August 2019
Received in revised form 7 January 2020
Accepted 9 January 2020
Available online 13 January 2020

Keywords:
Scandinavian Caledonides
Shoshonitic
Ultrapotassic
LREE enrichment
Beryllium
Thorium

ABSTRACT

Shoshonitic to ultrapotassic, mantle-derived volcanic rocks found within certain accretionary and collisional settings have trace element patterns comparable to those of common arc-related rocks, but with extreme enrichments in highly incompatible elements. Such rocks, previously unknown in the Scandinavian Caledonides, have been discovered in the Oppdal area in the Trondheim Nappe Complex, central Norway. The volcanic rocks are part of the Skarvatnet unit, which consists of (1) the Kinna volcanic succession, (2) the Storgruvpiken rhyolite, and (3) the Skaret conglomeratic succession. The Kinna volcanic succession is interpreted as consisting mainly of submarine pyroclastic flows. A trachytic bed from within this succession is dated to 474 ± 1 Ma. The Storgruvpiken rhyolite is interpreted as a shallow, subvolcanic intrusion or volcanic dome, and is dated to 470 ± 1 Ma. The Skaret conglomerates were deposited in a shallow-marine, tectonically active setting post-dating the Storgruvpiken rhyolite. The Kinna volcanic succession is highly enriched in Th, U, Pb and LREE, with trace element signatures remarkably similar to high-K to ultrapotassic rocks of the Alpine-Himalayan and other orogenic belts. By analogy with these recent examples, the Kinna volcanic succession is interpreted as the result of a two-stage process: (1) subduction and partial melting of continent-derived material caused extensive metasomatism of the overlying mantle wedge, (2) partial melting of this heterogeneous mantle source produced the highly enriched mantle melts. The Storgruvpiken rhyolite, particularly enriched in beryllium, is interpreted as the result of partial melting of Kinna-type rocks at depth. The Skarvatnet unit is interpreted as the result of a complex tectonic evolution at the margin of the Iapetus Ocean, involving the following stages: (1) intra-oceanic subduction, producing the Løkken-Vassfjellet-Bymarka ophiolite at 487–480 Ma, followed by (2) the arrival of the Laurentian margin or an associated micro-continent at ca. 480 Ma, leading to the subduction of large amounts of continent-derived material and subsequent metasomatism of the overlying mantle wedge, (3) arc-continent-collision and slab retreat/slab break-off, causing an intermittent phase of mantle-derived, highly enriched magmatism preserved as the Kinna volcanic succession and the Storgruvpiken rhyolite at 475–470 Ma.

1. Introduction

Magmatism above subduction zones is important for the growth of the continental crust and for refining its chemistry. This complex geological environment produces abundant highly evolved plutonic and volcanic rocks. Magmatic rocks with intermediate SiO_2 contents, primarily andesitic rocks, are considered to be the hallmark of subduction zone magmatism, while they are relatively rare in other geological settings. Typically, arc-related andesites are relatively enriched in large ion lithophile elements (LILE, e.g. K, Rb, Ba), light rare earth elements (LREE) and certain high field strength elements (HFSE) such as Th and U, with abundances commonly on the order of 10–100 x primitive mantle. These enrichments are generally accompanied by negative anomalies in Nb, Ta and Ti, with abundances of <10 x primitive mantle (e.g. Marschall and Schumacher, 2012; Pearce and Peate, 1995).

Some basaltic to intermediate volcanic rocks can be far more enriched in these incompatible elements (on the order of 100–1000 x primitive mantle), indicating a similar, but more extreme process of formation compared to the more common arc-related rocks. They are the product of potassic to ultrapotassic mantle-derived magmatism found in accretionary, collisional and post-collisional magmatic settings (e.g. Conticelli et al., 2009; Ersoy and Palmer, 2013; Peccerillo, 1999; Peccerillo and Martinotti, 2006).

* Corresponding author.
E-mail address: b.h.dalslaen@geo.uio.no (B.H. Dalslåen).

https://doi.org/10.1016/j.lithos.2020.105372

The enrichment of various elements in arc-related magmatic rocks is generally attributed to the transfer of these elements from subducted crustal material in the down-going slab into the overlying mantle, which then melts to produce arc magmas (e.g. Hermann and Rubatto, 2009; Plank and Langmuir, 1998; Spandler and Pirard, 2013; Tommasini et al., 2011). The details of such complex element transfers are still not fully understood and the budget for each of the enriched elements is probably controlled by several factors, including, e.g., the original composition of subducted sediments or continental crust, the type of reactions releasing fluids and partial melts from the subducting slab, the composition and mineralogy of the mantle and its reaction with the released fluids and melts, the mechanisms and degrees of partial melting of the mantle source and, ultimately, fractional crystallisation and assimilation processes during magma ascent.

In the case of extremely enriched, potassic to ultrapotassic mantle-derived rocks, a complex polyphase petrogenetic model is generally envisaged, with several stages of mantle metasomatism and enrichment prior to partial melting and magma formation (e.g. Conticelli et al., 2009; Peccerillo, 1999). This model involves K-rich melts or fluids derived from the subducted crustal material that react with the surrounding mantle to form plogophite-rich veins prior to partial melting. Mixing different proportions of magmas derived from the phlogopite-rich veins and the surrounding mantle might explain the range of observed rock types from ultrapotassic to shoshonitic and calk-alkaline (e.g. Foley, 1992a, 1992b; Förster et al., 2017). The mantle metasomatism is attributed to subduction processes, whereas the final partial melting of the enriched mantle is related to other tectonic processes such as slab roll-back and break-off, strike-slip faulting, or orogenic collapse and lithosphere delamination (e.g. Cheng and Guo, 2017; Ersoy and Palmer, 2013; Guo et al., 2014; Pe-Piper et al., 2009; Pérez-Valera et al., 2013; Prelević et al., 2008).

In this contribution we present field observations, geochemical and geochronological data from a hitherto unknown suite of Ordovician (c. 475–470 Ma) mafic, intermediate and felsic volcanic rocks from the Oppdal area in the central Scandinavian Caledonides (Fig. 1). These rocks have a geochemical signature that in many respects resembles that of typical arc settings, but with far stronger enrichments of elements like Th, U, Be and LREE, similar to potassic to ultrapotassic rocks of the Mediterranean area (e.g. Peccerillo, 1999). No similarly enriched, mafic to felsic volcanic rocks have been documented in the Scandinavian Caledonides so far. Younger, *syn-* to post-collisional (c. 430–400 Ma) shoshonitic and ultrapotassic rocks are documented by e.g. Thompson and Fowler (1986) from the Scottish Caledonides, and a c. 418 Ma ultrapotassic syenite is reported from the Appalachians (West et al., 2007). Similarly enriched rocks from the early, pre-collisional phase of Iapetus closure are extremely rare in the Caledonian orogen, with a c. 464–462 Ma shoshonitic monzogabbro in the Appalachians (Lissenberg et al., 2005) being the only described occurrence. Based on our new results we discuss potential petrogenetic models and tectonic implications for the subduction history of the Iapetus Ocean.

2. Geological setting

2.1. Subduction-related rocks within the central Scandinavian Caledonides

The Caledonian orogen represents a major continent-continent collision zone resulting from the closure of the Cambrian–Ordovician Iapetus Ocean and collision of the continents Laurentia and Baltica in Silurian times (e.g. Corfu et al., 2014; Roberts and Gee, 1985). Several subduction zones were probably active in the Iapetus Ocean, and volcanic rocks related to these subduction zones are preserved all along the orogenic belt (Fig. 1). The most prominent remnants of intra-oceanic Iapetus crust are Late Cambrian to Early Ordovician island-arc fragments and supra-subduction zone (SSZ) ophiolites (e. g. Grenne et al., 1999; Pedersen et al., 1992; Slagstad et al., 2014) (Fig. 1).

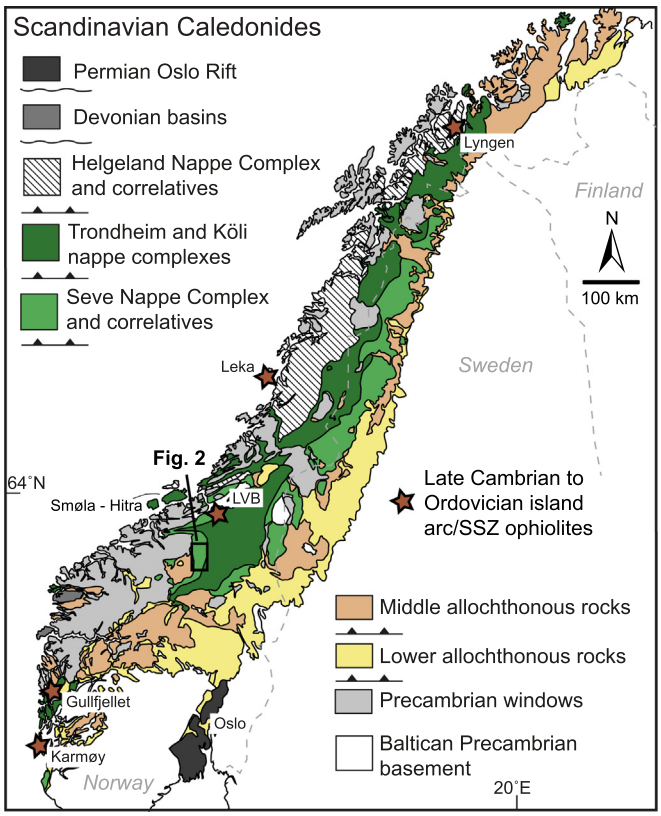

Fig. 1. Overview map of the Scandinavian Caledonides, with localities mentioned in the text.

The Trondheim Nappe Complex (TNC) of central Norway (Fig. 1) contains some of the best-preserved Iapetus-derived terranes within the Scandinavian Caledonides (Grenne et al., 1999; Slagstad et al., 2014). Within the western TNC, oceanic crust is represented by the 487 to 480 Ma Løkken–Vassfjellet–Bymarka (LVB) ophiolite fragments (Fig. 1), comprising gabbros, sheeted dykes and pillow lavas (Grenne et al., 1999; Slagstad et al., 2014). The LVB ophiolite is interpreted to have formed over an intra-oceanic subduction zone, and was obducted onto a continental margin between 478 Ma and 468 Ma as constrained by the last recorded magmatic activity within the ophiolite and the first post-obduction magmatism (e.g. Slagstad et al., 2014). Obduction and erosion were followed by deposition of the sedimentary and volcanic rocks of the Hovin and Horg Groups (Vogt, 1945). The Hovin Group contains the Hølonda Porphyrites, a shoshonitic volcanic and subvolcanic suite with geochemical signatures that were interpreted by Grenne and Roberts (1998) as indicating formation in a continental arc setting. The absolute age of the Hølonda Porphyrites is unknown, but they are associated with richly fossiliferous sediments of Late Arenig/Early Llanvirn (Middle Ordovician, ca. 468–465 Ma) age that show an unequivocal Laurentian faunal affinity (e.g., Bruton and Bockelie, 1980). The Early to Middle Ordovician arc volcanism represented by the SSZ ophiolites and the Hølonda Porphyrites was succeeded by arc type magmatism in the Late Ordovician to Silurian, represented in the central Scandinavian Caledonides by e.g. the Smøla-Hitra batholith (ca. 445–440 Ma; Tucker et al., 2004). This magmatism was followed in the Silurian by widespread mafic intrusives, including the Innset massif of the Oppdal area (Fig. 2; Nilsen et al., 2003), reflecting short-lived extension prior to the main Caledonian continental collision (Slagstad and Kirkland, 2018).

2.2. Geology of the Oppdal area

The area investigated in this study is located in a late/post-Caledonian half-graben structure in the south-western part of the TNC

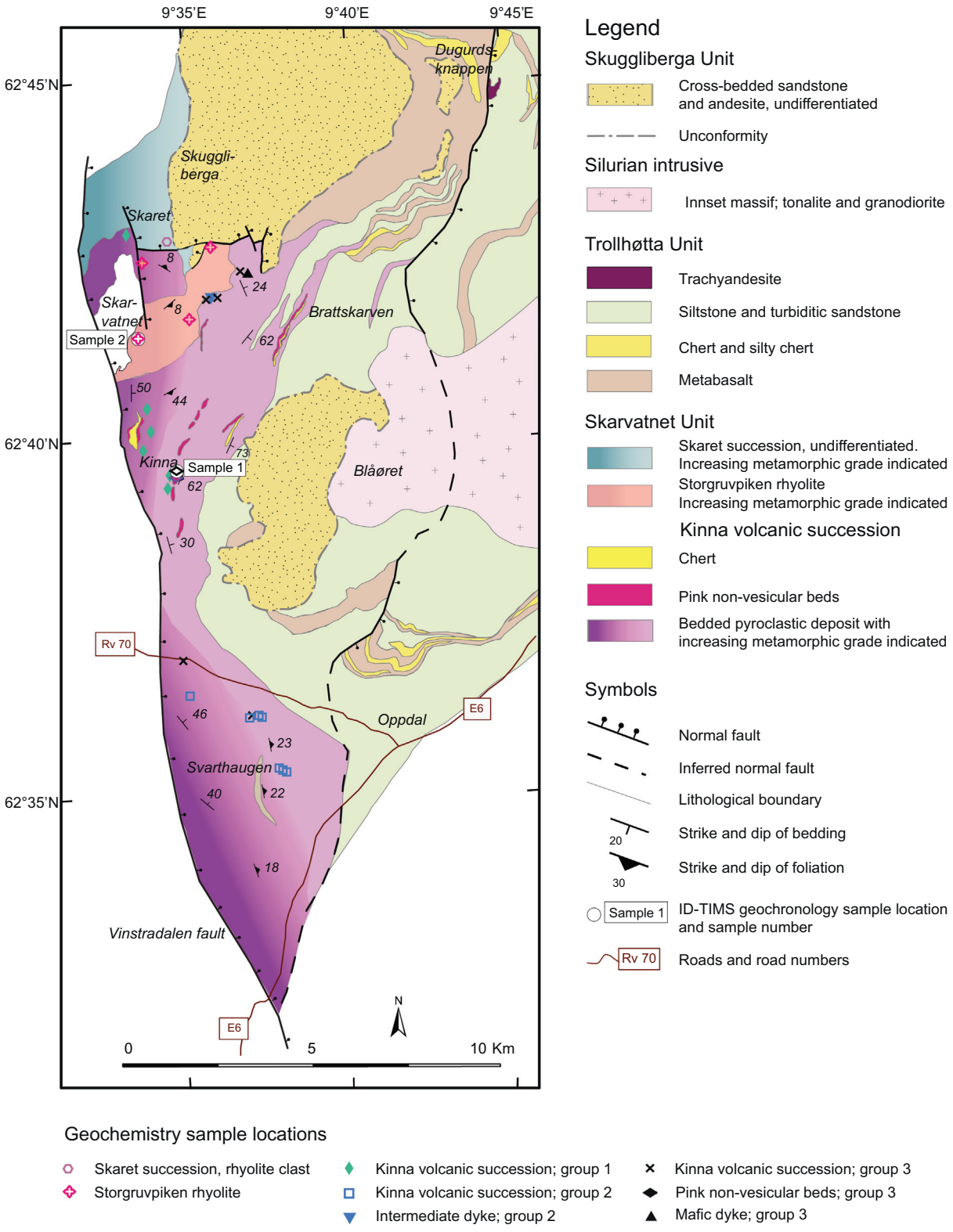

Fig. 2. Geological map of the study area with sample localities; the symbols correspond to those of Figs. 7–10.

(Figs. 1, 2), separated from the underlying, higher-grade nappes by the Vinstradalen fault (Fig. 2). The rocks of the area are generally moderately deformed with an *E*-dipping regional foliation and are metamorphosed to greenschist facies. Towards the Vinstradalen fault, they grade into amphibolite facies, strongly foliated rocks (Fig. 2). On the 1:250000 scale bedrock map of Nilsen and Wolff (1989), the rocks investigated in the present study were mapped as volcanic breccias, siltstones and greywackes interlayered with rhyolite. In some literature these relatively low-grade rocks have been referred to as the Tronget unit (e.g., Gee et al., 1985), a loose term originally introduced by Krill (1980) for rocks farther south. Recent, detailed work by Stokke et al. (2018) around Dugurdsknappen (Fig. 2) defined a sequence of E-MORB basalts, chert, cherty siltstone and turbiditic sandstone, referred to in the following as the Trollhøtta unit, which was isoclinally folded

and unconformably overlain by Silurian sandstones and calc-alkaline volcanic rocks of the Skuggliberga unit (Fig. 2).

3. Results

3.1. Field relations

We remapped the volcanic breccia/siltstone/greywacke and rhyolite units of Nilsen and Wolff (1989), which stretch from south of Oppdal northwards to Skaret, covering an area of approximately 60 km^2 (Fig. 2). These rocks, here collectively referred to as the Skarvatnet unit, were subdivided into three different rock associations. These are (1) the Kinna volcanic succession, including associated dykes and minor intercalated chert, (2) the Storgruvpiken rhyolite, and (3) the sedimentary Skaret succession (Fig. 2). Primary macrostructures are generally well preserved, particularly within the pressure shadow of the Storgruvpiken rhyolite. However, metamorphism and regional-scale deformation have partly erased small-scale primary textures. All three associations have undergone regional metamorphism, but the prefix 'meta' is omitted in the following descriptions and discussions for simplicity.

3.1.1. The Kinna volcanic succession

The c. 2.5 km thick Kinna volcanic succession is the most voluminous of the three units, covering an area of approximately 40 km^2 (Fig. 2). It is mostly bedded, with up to 5 m thick, light- to medium-grey fragment-bearing beds alternating with finer grained, fragment-free beds of similar composition (Fig. 3a). The boundaries between the beds are sharp, and grading or other way-up criteria have not been observed. In some areas the rocks have experienced bedding-parallel tectonic flattening (Fig. 3a) whereas others are virtually undeformed (Fig. 3b). The fragment-bearing beds consist of either scattered fragments (Fig. 3b) or densely packed fragments (Fig. 3c, d) in a fine-grained matrix. The fragments are angular to rounded and fragment size is highly variable; 10–50 cm is most common but fragments up to 1.5 m have been observed. There is no systematic variation in grain or fragment size within individual beds. Crusted fragments are observed (Fig. 3e). Towards the Vinstradalen fault (Fig. 2) the Kinna succession occurs as alternating beds of biotite–amphibole–quartz schists and more gneissic-looking, strongly deformed fragment-bearing beds (Fig. 3d). Towards the northeast, the Kinna volcanic beds are intercalated with metabasalts, cherts and siltstones of the Trollhøtta unit; minor chert layers also occur within the western part of the Kinna succession (Fig. 2).

The fragments within the bedded Kinna succession are dominated by feldspar, fine-grained dark mica (partly replaced by chlorite), epidote and carbonate minerals. Porphyritic fragments are abundant, with dark green to black, 2–10 mm phenocrysts of euhedral amphibole commonly replaced by a fine-grained aggregate of dark mica, chlorite and epidote (Fig. 3f-h). Some dark mica that forms euhedral hexagonal crystals 2–4 mm across is also considered a primary magmatic phase. Most fragments are vesicular with the vesicles ranging from 0.5 mm to 3 mm and constituting up to 50% by volume. Vesicle shape vary from spherical to elongate; vesicles are filled with carbonate, quartz or feldspar (Fig. 3i), the latter two locally forming a thin outer rim of the vesicles (Fig. 3j). Some elongated and densely packed fragments still have spherical vesicles, demonstrating that fragment flattening is a primary feature at least locally. Unequivocal evidence of welding is not observed but cannot be ruled out. The fine-grained beds and the matrix between fragments consist of a homogenous, fine-grained assemblage of epidote, chlorite, biotite, feldspar, calcite, magnesite and minor quartz.

The central part of the Kinna volcanic succession locally contains fine-grained, non-vesicular, volcanic rocks characterized by a light pinkish colour (pink non-vesicular beds, Kinna group 3 in Fig. 2; Fig. 3k). These volcanic rocks are up to 60 m thick. Individual outcrops are up to 300 m along strike and their linear arrangement indicates that they occur mainly at two stratigraphic levels (Fig. 2). These rocks contain abundant fine-grained K-feldspar and consist of fine-grained, non-vesicular, densely packed subangular to angular fragments of a few millimetres to 3 cm in size (Fig. 3l). The fragment size is substantially smaller than in the bedded Kinna volcanic succession.

Close to the Storgruvpiken rhyolite, the Kinna volcanic succession is cut by several parallel, up to 2 m thick, fine- to medium-grained intermediate dykes with chilled margins (intermediate dyke, Kinna group 2 in Fig. 2; Fig. 4a). The centres of the dykes have a porphyritic texture, where K-feldspar laths up to 3 cm are partly aligned with the margins of the dykes (Fig. 4b); the groundmass has a trachytic texture dominated by fine-grained alkali feldspar (Fig. 4c). Farther north, a mafic dyke with scattered, 2–3 mm amphibole phenocrysts in a fine- to medium-grained biotite-rich matrix cuts the Kinna volcanic succession (Mafic dyke, Kinna group 3 in Fig. 2). The relationship between the dykes and the Storgruvpiken rhyolite is uncertain due to lack of exposure.

3.1.2. The Storgruvpiken rhyolite

The bedding of the Kinna volcanic succession is cut to the northwest by the Storgruvpiken rhyolite, an elongate body oriented approximately NNE–SSW that covers approximately 2.5 km^2 (Fig. 2). The rhyolite body contains large (up to 10 m) xenoliths of Kinna rocks (Fig. 5a). The Storgruvpiken rhyolite is a very fine-grained, grey to light pinkish rock almost devoid of mafic minerals; only few, small biotite grains and opaques are present. Euhedral phenocrysts of millimetre-size alkali feldspar are observed in thin section at several localities (Fig. 5b). Some parts of the rhyolite are massive with no internal structure. Other parts show millimetre-thick planar features interpreted as primary igneous flow-banding with an orientation different from the regional foliation and the bedding of the Kinna volcanic rocks (Fig. 5c). Millimetre- to centimetre-size angular fragments in a darker, finer grained matrix occur locally (Fig. 5d).

3.1.3. The Skaret succession

The area to the north of the Kinna volcanic succession is dominated by different conglomerates and clastic sedimentary rocks, here referred to as the Skaret succession (Fig. 2). Conglomerates constitute approximately 60% of the rocks in the area. Three main types of conglomerates were observed.

(1) The most abundant type is a polymict conglomerate with a calcareous, biotite-rich greywacke matrix. The clast material is highly diverse; felsic/intermediate and mafic volcanic rocks, siltstone, sandstone, jasper, chert, fine-grained marble and clasts of Kinna-type volcanic rocks have been observed. The clasts are angular to subrounded, ranging in size from pebble to meter-sized boulders; the largest blocks consist of immature sandstone and fine-grained marble and are up to 1.5 m across (Fig. 6a). This conglomerate is associated with thick-bedded to laminated calcareous greywacke (Fig. 6b), marble beds and monomict marble conglomerate.
(2) A different conglomerate is characterized by abundant fine-grained, pink felsic or intermediate volcanic clasts mostly <30 cm; clasts up to 1 m are also found. The shape of the clasts is highly diverse; sub-angular clasts are most common. Local medium-grained mafic clasts are up to 70 cm and are more rounded than the felsic/intermediate ones. The conglomerate is clast-supported, and the clasts are embedded in a very fine-grained, biotite- and chlorite-rich matrix.
(3) The third type of conglomerate consists almost exclusively of angular metabasaltic fragments (1–5 cm), with subordinate pink, fine-grained felsic/intermediate volcanic clasts and small grains of jasper set in an epidote-rich matrix (Fig. 6c).

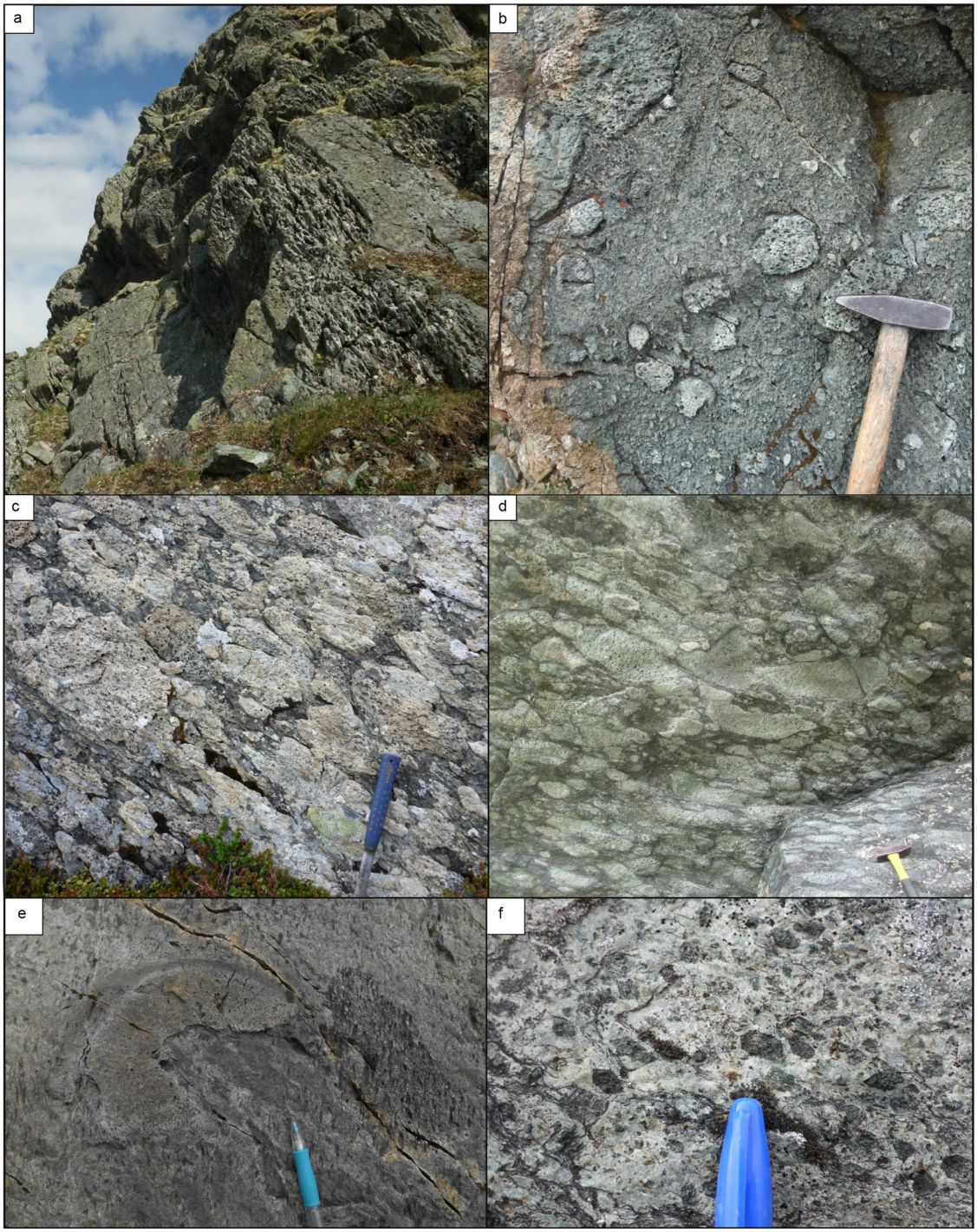

Fig. 3. Field and thin section photographs of the Kinna volcanic succession. a Alternating fragment-bearing and fragment-free beds. b Scattered, vesicular volcanic fragments in fine-grained matrix of similar composition; black spots are aggregates of biotite and chlorite that replace amphibole phenocrysts. c Densely packed, angular volcanic fragments. d Densely packed fragments within a biotite-rich matrix (amphibolite facies, close to the Vinstradalen fault). Kinna volcanic succession continued. e Broken fragment of a rounded, partly crusted fragment in a grey matrix with biotite-chlorite aggregates probably replacing amphibole; the crust and rounded shape suggest this is a fragment of a volcanic bomb. f Euhedral phenocrysts of amphibole replaced by aggregates of dark mica and chlorite. g Thin section photo from a basaltic fragment (Kinna group 1), with an amphibole phenocryst partly replaced by dark mica and chlorite. Plane polarized light. h Thin section photo of dark mica – chlorite aggregate completely replacing euhedral, rhomb-shaped mineral, probably amphibole. Plane polarized light. i Fragment with spherical vesicles partly filled with quartz, carbonate and/or feldspar. j Thin section photo from a fine-grained trachyandesitic rock (Kinna group 3) with a vesicle filled with a quartz – feldspar rim and carbonate core. Crossed polars. k Non-vesicular pink volcanic rock that locally occurs interbedded within the fragment-bearing Kinna volcanic succession. Phenocrysts are mainly K-feldspar; mafic minerals are only a minor constituent (the dark spots are lichen). l Thin section photo of the non-vesicular pink volcanic rock, with fine-grained partly flattened fragments and minor dark mica. Plane polarized light.

All three conglomerate types are interbedded with greenish, biotite-rich bedded immature sandstones with no internal grading, grey calcareous greywackes, and minor chert and marble. Slump folds and other soft-sediment deformation structures are common (Fig. 6d), and lithological boundaries within the succession are commonly distorted and/or truncated by other lithologies.

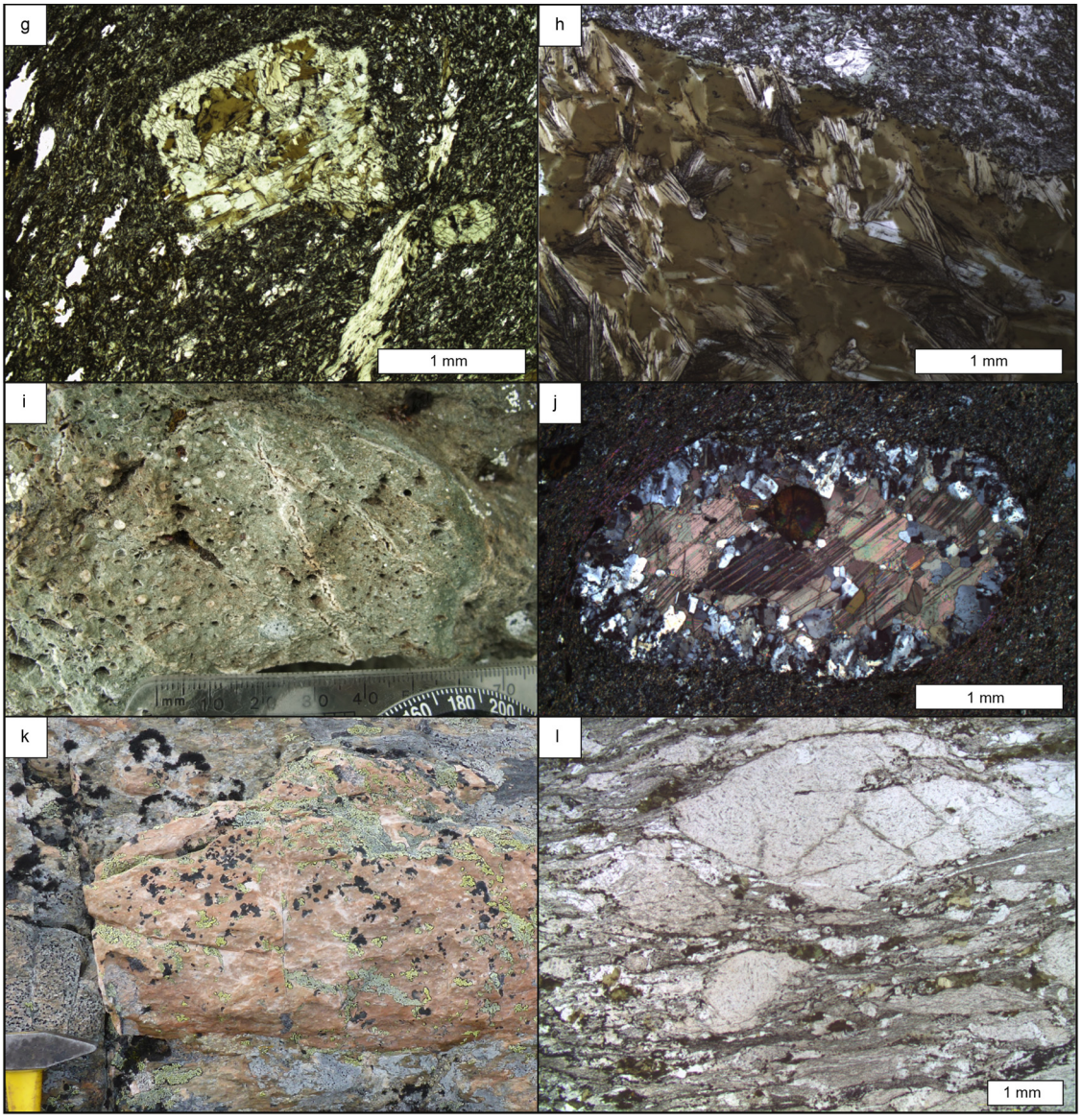

Fig. 3 (*continued*).

3.2. Geochemistry

3.2.1. Sampling and analytical procedure

We analysed 27 samples from the Skarvatnet Unit for major and trace elements. Sample localities are shown in Fig. 2. Samples with very high contents of phenocrysts and >5% vesicles were avoided. All samples were analysed at the Geological Survey of Norway, Trondheim. Major elements were analysed by X-ray fluorescence (XRF) spectrometry on glass beads fused with lithium tetraborate, and trace elements were analysed by XRF spectrometry on pressed powder. Rare Earth Elements (REE) were analysed by inductively coupled plasma – mass spectrometry (ICP-MS) on the same glass bead used for XRF major element analysis. Common international standards were followed for all methods; details on standards and methods can be provided on request. The results are reported in Table 1 and in Figs. 7–10.

Eighteen of the samples are from the typical bedded Kinna volcanic succession. Eleven of these are fragments, five are from fine-grained fragment-free beds, and two are from the matrix of fragment-bearing beds. Two samples are from the pinkish, non-vesicular volcanic rocks in the Kinna volcanic succession. One sample is from an intermediate dyke and one from the mafic dyke in the Kinna volcanic succession. Four samples are from the Storgruvpiken rhyolite, and one is a rhyolite clast from the type 2 conglomerate of the Skaret succession (Fig. 2; Table 1).

3.2.2. The Kinna volcanic succession

The samples from the Kinna volcanic succession represent a spectrum of geochemical compositions which we have separated into three different groups based on specific geochemical features (Figs. 7–10). These three groups are not distinguishable in the field. Their random geographic distribution (Fig. 2) does not reveal any systematic age relationship, and we interpret them to be broadly coeval. Due to mobility of alkalies in the standard TAS diagram, we apply the Zr/Ti vs. Nb/Y diagram of Pearce (1996) for a general classification or our rocks (Fig. 7a). Kinna group 1 samples are subalkaline basaltic andesites and andesites, whereas Kinna group 2 and 3 samples are alkaline rocks ranging from trachyandesite to alkali rhyolite (Fig. 7a). All three groups are strongly enriched in most incompatible high field strength elements (HFSE), including the light rare earth elements (LREE), relative to continental crust and common oceanic or continental arc-related rocks (Table 1; Fig. 7b) (Pearce, 2008; Pearce and Peate, 1995; Rudnick and Gao, 2003). All three groups have relatively high contents

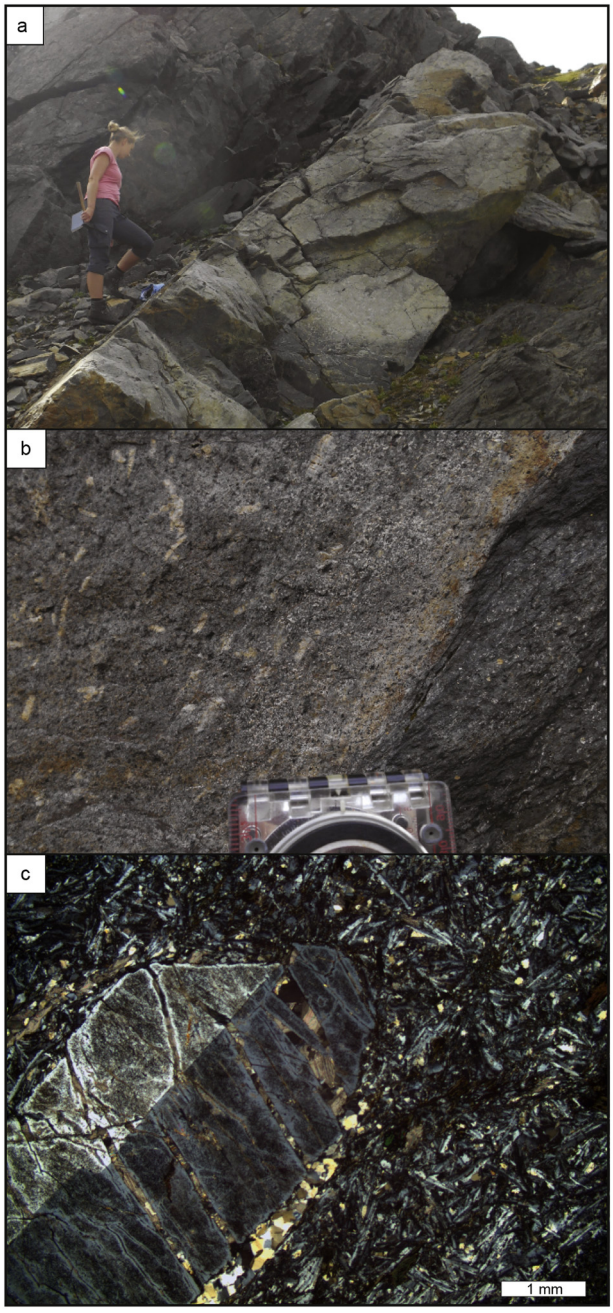

Fig. 4. a Trachytic dyke cutting the Kinna volcanic succession. b Contact between dyke and Kinna volcanic succession, with increasing grain size away from the chilled margin. Alkali feldspar phenocrysts are partly aligned with the dyke margin. c Thin section photo of simple twinned alkali feldspar phenocryst in a fine-grained alkali feldspar-dominated matrix. Crossed polars.

of MgO (up to 11 wt%; 5 samples have Mg# >70), Cr (up to 792 ppm) and Ni (up to 300 ppm), and even intermediate volcanic rocks can have concentrations of Cr up to 378 ppm at 57.1% SiO_2 (Table 1).

The SiO_2 vs. K_2O plot (Fig. 7c) must be considered with care in view of the potential mobility of potassium during sea-floor alteration and regional metamorphism; however, it is noteworthy that many Kinna samples have elevated K_2O values comparable to High-K calc-alkaline, shoshonitic and even ultrapotassic rocks. Although potassium values are obviously not reliable at individual sample level and some Kinna rocks may have experienced gross K_2O loss, several samples classify as ultrapotassic also based on the commonly used criteria of Foley et al. (1987): K_2O > 3 wt%, MgO > 3 wt%, K_2O/Na_2O > 2 (Table 1).

The basaltic-andesitic to andesitic Kinna group 1 samples have SiO_2 vs. K_2O contents comparable to high-K calc-alkaline to shoshonitic rocks (Fig. 7c). They are relatively rich in Th (9.5–48.1 ppm; the group 1 samples have an average Th content of 101 x N-MORB – this and all following values are averages compared with the mean N-MORB composition given in Gale et al., 2013), U (3.3–9.9 ppm; on average 70 x N-MORB,), Pb (11.9–36.5 ppm; on average 38 x N-MORB), and LREE (La on average 15 x N-MORB, Ce on average 11 x N-MORB). They have large negative Nb—Ta and Ti anomalies and exhibit a minor trough at Zr—Hf in the N-MORB-normalised multielement plot (Table 1 and Fig. 8a). Chondrite-normalised REE patterns (Fig. 8b) are steep (La_N/Lu_N = 16.8–34.9), showing an even slope towards the heavy REE (HREE) and minor negative Eu anomalies (0.71–0.85). Kinna group 1 samples contain up to 417 ppm Cr and 117 ppm Ni (Table 1), with a steep negative correlation between Zr and Cr (Fig. 9). Sm/La values are mostly <0.2, and the samples plot close to the estimated average upper crust (UC, Rudnick and Gao, 2003) and the estimates for Global Subducting Sediment (GLOSS, Plank and Langmuir, 1998) in a Sm/La vs. Th/La plot (Fig. 10).

The trachytic to alkali-rhyolitic Kinna group 2 samples, including the intermediate dyke, are even more enriched in Th (43.9–117 ppm; on average 284 x N-MORB), U (11.8–26.6 ppm; on average 227 x N-MORB), Pb (30.2–80.3 ppm; on average 91 x N-MORB), LREE (La on average 28.45 x N-MORB, Ce on average 20 x N-MORB), Be (1.4–44.9 ppm; on average 20 x N-MORB), and Zr (594–1060 ppm; on average 8 x N-MORB) (Table 1 and Fig. 8c). Compared to Kinna group 1 rocks they also have significantly higher Ta/La and Th/La ratios and lack the minor Zr—Hf trough (Fig. 8c). Chondrite-normalised REE patterns (Fig. 8d) have a very steep slope (La_N/Lu_N = 32.4–53.0), especially among the MREE, and have a slightly flatter trend among the HREE. Increasing SiO_2 with Zr is accompanied by decreasing MgO, P_2O_5 and Cr (Fig. 9a–c), suggesting that much of the group-internal variation can be attributed to fractional crystallisation of mafic phases and apatite. Similarly, a fairly wide range of negative Ti anomalies (Fig. 8c) and the Eu anomalies of 0.54–0.67 (Fig. 8d) likely reflect fractionation of titaniferous oxides and feldspar, respectively. Kinna group 2 samples have Sm/La ratios similar to those of Kinna 1, close to UC and GLOSS in the Sm/La vs Th/La plot (Fig. 10). They generally resemble shoshonitic to ultrapotassic rocks in the K_2O vs. SiO_2 diagram (Fig. 7c); the very low K_2O of three samples is considered to result from seafloor weathering, hydrothermal alteration and/or regional metamorphic processes in view of (1) their stable trace element patterns that are identical to other Kinna 2 samples and (2) the typical enrichment of K_2O along with Th and other highly incompatible elements in magma-forming processes in general (Hastie et al., 2007; Pearce and Peate, 1995).

The trachyandesitic Kinna group 3 samples, including the mafic dyke and the pink non-vesicular volcanic rocks, plot as shoshonitic to ultrapotassic (Fig. 7c). Their trace element patterns (Fig. 8e) generally follow those of Kinna group 2, although with even higher values of Th (53–192 ppm, on average 114 x N-MORB), U (12.9–30.2 ppm, on average 22 x N-MORB), Pb (50–299 ppm, on average 118 x N-MORB), Be (7.1–60.1 ppm, on average 21 x N-MORB) and Zr (410–1130 ppm, on average 703 x N-MORB). A moderately negative Eu anomaly of 0.52–0.74 is comparable to that of Kinna 2 (Fig. 8f). A notable difference, however, is a peculiar, convex upward pattern at the La—Sm part of the chondrite-normalised REE diagram (Fig. 8f). Accordingly, Kinna group 3 samples have significantly higher Sm/La ratios (>0.2) than those of the other Kinna samples, plotting towards the Samarium – Lanthanum – Thorium (SALATHO) end-member of Tommasini et al. (2011) on the Sm/La vs. Th/La diagram (Fig. 10).

3.2.3. The Storgruvpiken rhyolite

The Storgruvpiken samples, including the clast from the Skaret conglomerate, are highly evolved, peraluminous and A-type alkaline rhyolites (Fig. 7a). They share many of the geochemical characteristics with the Kinna group 2 and 3 samples, but are even more enriched in Th

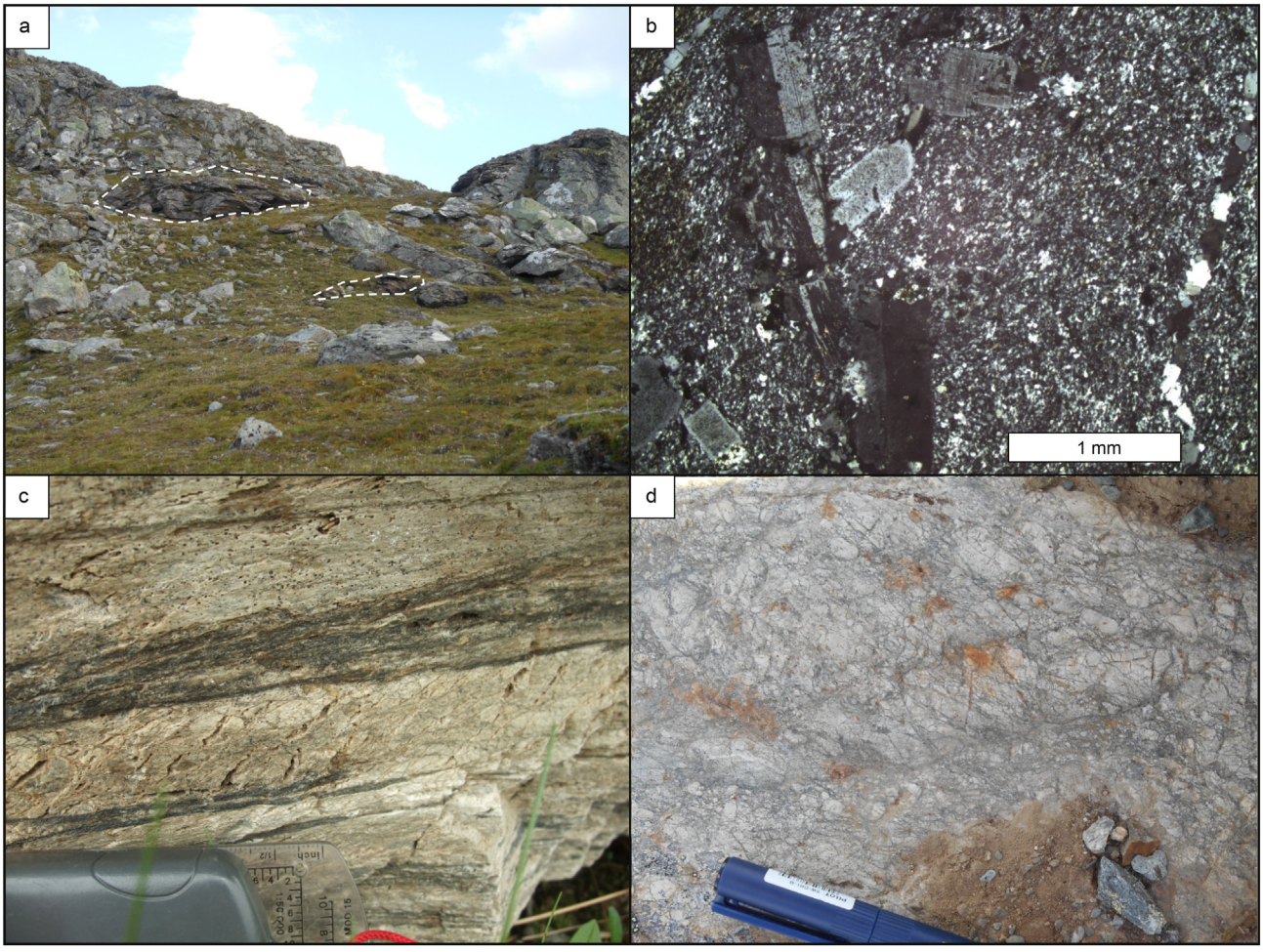

Fig. 5. Storgruvpiken rhyolite. a Massive rhyolite with large rafts of darker Kinna volcanic rocks (white outline). b Thin section photo from the Storgruvpiken rhyolite; subhedral phenocrysts of alkali feldspars with no, simple and gridiron twinning set in a fine-grained matrix. Crossed polars. c Rhyolite flowbanding. d Rhyolite with small, angular fragments embedded in a fine-grained light-grey matrix.

(113–278 ppm, on average 175 x N-MORB) and U (23.0–61.8 ppm, on average 42 x N-MORB) and have somewhat lower contents of LREE (La on average 15 x N-MORB; Ce on average 13 x N-MORB), Zr (329–530 ppm, on average 425 x N-MORB) and Hf (11.4–24.7 ppm, on average 7 x N-MORB) (Table 1, Fig. 8g). Notably, Be is extremely enriched in some samples (6.7–66.5 ppm; on average 38 x N-MORB, Table 1). Th/Ta ratios are similar to those of Kinna 2 and 3, but the generally lower concentrations of LREE produce a less pronounced trough at Ta—Nb (Fig. 8g). REE-patterns (Fig. 8h) have a significantly gentler slope than the Kinna 2 and 3 rocks (La_N/Yb_N 9.4–17.0), partly overlapping with Kinna 1 patterns (La_N/Lu_N 16.8–34.9). Compared to the Kinna volcanic succession, the more evolved Storgruvpiken rhyolite has much larger negative Ti and Eu (0.02–0.17) anomalies (Fig. 8g–h).

3.3. Geochronology

3.3.1. U—Pb TIMS method

Two samples were crushed, and heavy minerals were separated by standard magnetic and heavy liquid techniques at the University of Oslo. Selected zircons from sample 1 were annealed for ca. 72 h at 900 °C and chemically abraded with HF (+HNO_3) at 195 °C for 14 h (Mattinson, 2005). The high-U zircons from sample 2 were air abraded (Krogh, 1982) because of advanced metamictization. After optical inspection, euhedral high aspect ratio (>1:4) zircon grains were chosen for analysis, spiked with a mixed ^{202}Pb–^{205}Pb–^{235}U tracer that has recently been calibrated to the EARTHTIME (ET) 100 Ma solution (Svensen et al., 2015), and dissolved in HF (+HNO_3) at ca. 210 °C for >48 h in Teflon micro capsules and a Parr type bomb. All dissolved grains subsequently went through column chemistry in order to separate U and Pb from potentially interfering and ionization inhibiting elements (Krogh, 1973). Details of the general mass spectrometric techniques and parameters used are presented in Augland et al. (2010) with upgraded laboratory parameters: Pb blank generally <1 pg with a composition of $^{206}Pb/^{204}Pb = 18.04 \pm 0.40$; $^{207}Pb/^{204}Pb = 15.22 \pm 0.30$; $^{208}Pb/^{204}Pb = 36.67 \pm 0.50$; improved precision of fractionation on U and Pb fractionation parameters of 0.02% and down to 0.003% 1σ for U and Pb, respectively. Reduction of raw data was conducted using Tripoli (Bowring et al., 2011) and analytical errors and corrections (including common Pb, fractionation corrections and Th corrections, assuming Th/U in the magma of 3) were incorporated and propagated in the Excel macro based on the algorithms published in Schmitz and Schoene (2007). Ages were calculated by the use of the ISOPLOT Excel macro of Ludwig (2003) using the decay constants of Jaffey et al. (1971) and are presented in Fig. 11 and Table 2.

3.3.2. Results U—Pb TIMS dating

3.3.2.1. Sample 1 (15BD_256; UTM (32) 529655/6947568). Sample 1 is from a pink non-vesicular volcanic bed within the Kinna succession (Fig. 2), which shows a trachytic composition belonging to Kinna group 3 (Figs. 7-10). Four clear, colourless to slightly yellow zircon fragments were analysed. All analyses are concordant and overlapping, giving a weighted mean $^{206}Pb/^{238}U$ age of 474 ± 1 Ma (2σ; MSWD = 1.8) (Fig. 11a; Table 2).

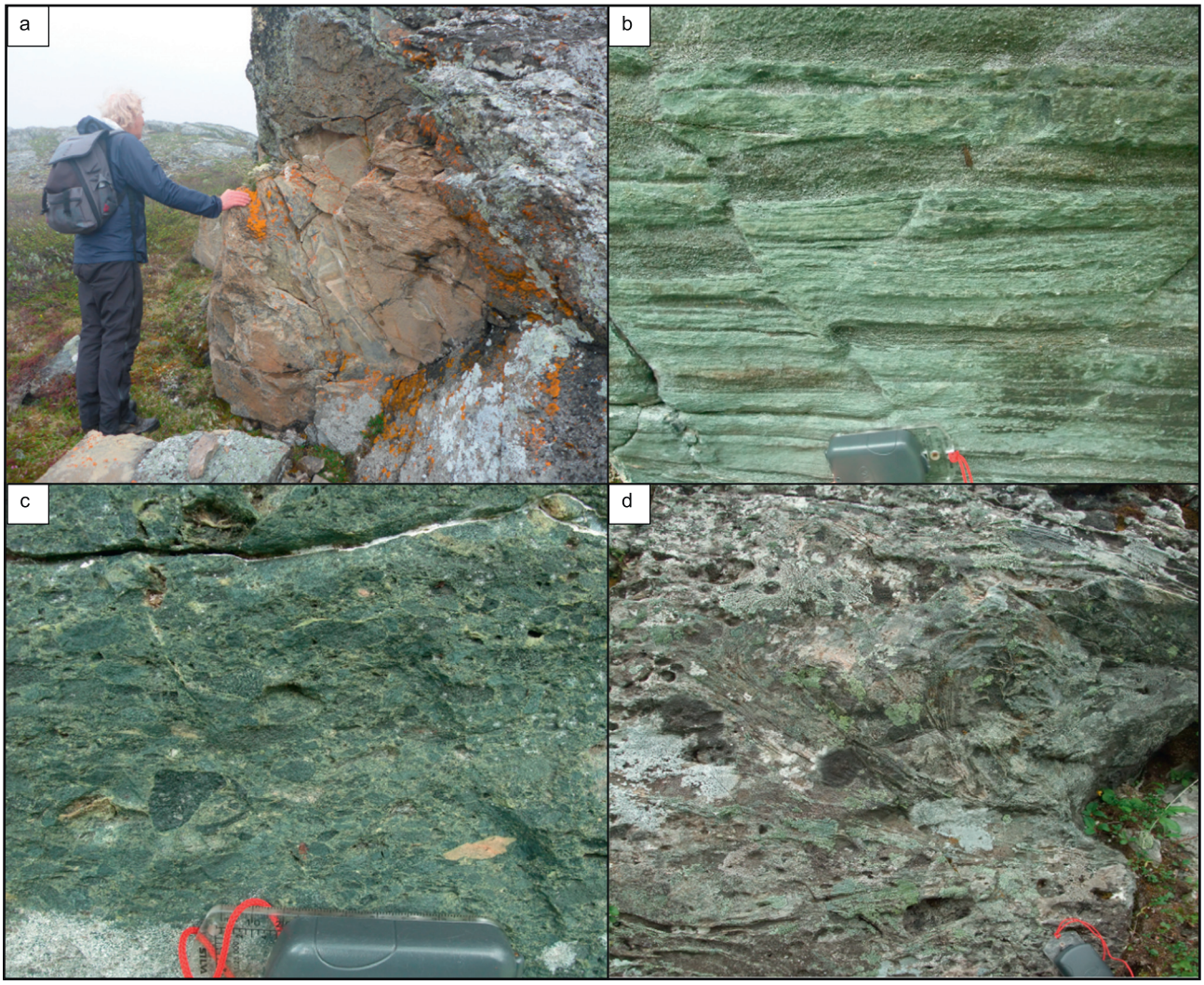

Fig. 6. The Skaret succession. a Large, angular block of fine-grained marble in a greywacke matrix. b Green, bedded sandstone with biotite-rich layers. Carbonate clasts are weathered out. c Angular basaltic and felsic volcanic fragments in an epidote-rich matrix. d Polymict conglomerate with calcareous, biotite-rich greywacke matrix, disturbed by slump folding.

3.3.2.2. Sample 2 (TGR12–739; UTM (32) 528662.6951317). Sample 2 is from the Storgruvpiken rhyolite (Fig. 2). In this area the rhyolite has a fragmental texture with planar features interpreted to be related to movement of viscous magma. Zircon occurs as euhedral, mostly brown and opaque, equant crystals dominated by {100} and {101} crystal faces. Inferred cores are seen in some grains, but they are rare and such grains were avoided during selection. Three zircons, one pink and two brown grains were analysed and are all concordant. The weighted mean $^{206}Pb/^{238}U$ age is 470 ± 1 Ma (2σ; MSWD = 1.3) (Fig. 11b; Table 2).

4. Discussion

4.1. Depositional setting of the Skarvatnet unit

4.1.1. The Kinna volcanic succession

The fairly uniform mineralogical and geochemical composition of the Kinna volcanic succession indicates that these deposits had little input from non-volcanic sources. In addition, the lack of graded beds, erosional channels or other sedimentary features typical of clastic sedimentation in water rules out re-deposition of volcanic rocks as clastic debris flows. Hence, we consider it most likely that the Kinna succession represents primary volcanic deposits. The alternation of beds with and without fragments shows that similar processes occurred repeatedly, probably with similar intensities in each cycle since the beds typically have a restricted thickness ranging from 50 to 100 cm. Several eruptive pulses capable of producing the variation in fragment amount are considered more likely than repeated erosional and clastic depositional processes, which would probably lead to more variation in bed thickness and content. Possible volcanic deposit types discussed in the following include lava flows, lahars, pyroclastic flows and ash fallouts.

An origin as individual lava flows where fragment-free portions are central parts and fragment-bearing portions represent auto-brecciated upper parts of flow units is considered unlikely as the fragments within one bed have a large variation in content of phenocrysts. Subrounded fragments are also not typical for auto-brecciation. The pink non-vesicular beds in contrast, with their internal small-scale fragmentation, might possibly represent felsic lava flows with limited extent, although other origins cannot be ruled out.

The unsorted nature of the fragment-bearing beds of the Kinna volcanic succession could result from several types of debris flow; lahars and pyroclastic flows (subaerial or submarine) being the most relevant. There are no single features that can distinguish between unwelded pyroclastic deposits and lahars (Fisher and Schmincke, 1984), but since pumice and highly vesicular material is more common in pyroclastic flows than in lahars, it is considered more likely that the Kinna succession represents pyroclastic flow deposits.

Table 1
Major and trace element analyses. Elements in italics are analysed on ICP-MS, other elements are analysed on XRF. * = W analysed on XRF. Mg# = 100xMg/(Mg + Fe). RG-2003 are estimates for average continental crust composition from Rudnick and Gao (2003).

Group	Kinna volcanic succession group 1						Kinna volcanic succession group 2							
Sample	15BD_1471	15BD_249	15BD_259	15BD_306	17BD_43	BD15_538	15BD_1061	17BD_39	17BD_41A	17BD_41B	17BD_42C	BD15_272	BD15_273	17BD_67
SiO_2%	46.4	54.2	57.5	48.3	48.4	54.9	58.3	57.1	51.6	49.7	48.5	63.3	67.7	59.5
Al_2O_3	13.2	16.8	14.2	13.3	15.6	14.6	16.0	19.0	15.1	14.6	13.5	16.7	15.6	16.6
Fe_2O_3	6.88	10.1	5.20	10.8	10.1	6.85	3.82	4.55	6.92	6.53	6.89	4.05	1.07	3.61
TiO_2	0.739	0.686	0.748	0.604	0.693	0.591	0.372	0.973	0.781	0.986	0.942	0.338	0.253	0.657
MgO	8.98	1.84	3.07	9.98	8.46	7.04	3.40	2.49	7.09	9.08	9.83	1.07	0.209	2.28
CaO	12.4	3.52	7.40	7.15	8.75	7.56	6.10	2.23	5.30	7.41	8.00	5.29	3.35	1.86
Na_2O	1.76	6.54	4.24	1.31	2.94	4.28	7.43	3.35	4.28	1.29	1.13	6.78	8.45	1.46
K_2O	2.57	2.68	1.76	3.68	1.76	1.82	0.79	5.89	3.74	5.21	5.00	0.60	0.37	11.0
MnO	0.164	0.108	0.070	0.142	0.152	0.116	0.066	0.048	0.076	0.100	0.116	0.045	0.083	0.045
P_2O_5	0.433	0.601	0.562	0.331	0.366	0.417	0.152	0.328	0.469	0.608	0.535	0.184	0.197	0.317
LOI	4.93	2.04	4.33	3.14	2.12	1.30	2.51	2.38	2.92	3.23	4.04	1.15	1.84	1.76
Ba ppm	2880	680	712	1080	630	476	308	1470	902	3080	2420	82	59	1430
Co	31.1	21.5	29.4	45.9	39.1	25.8	10.2	13.4	27.2	32.2	38.3	9.9	<4	11.1
Cr	170	18.0	205	399	228	290	50.1	378	443	268	658	18.9	51.4	88.3
Cu	99.8	50.4	36.4	236	91.2	11.8	147	29.4	44.9	128	124	6.5	14.3	7.0
Ga	11.5	11.9	10.9	13.5	15.5	11.2	8.40	23.2	19.5	19.9	16.8	12.2	5.10	23.9
Ni	106	45.3	74.2	108	79.5	115	34.3	47.5	163	201	244	43.0	<5	34.2
Pb	16.1	36.5	18.3	15.5	18.1	11.9	80.3	30.2	37.3	51.7	22.1	48.8	39.6	62.5
Rb	81.0	77.9	78.8	148	74.5	67.4	30.8	219	223	213	215	24.9	7.0	455
Sc	24.7	8.0	27.1	28.0	34.4	27.7	8.6	21.8	21.8	22.5	34.1	<5	<5	14.7
Sn	<5	<5	<5	<5	<5	<5	6.00	8.70	13.1	12.6	10.4	12.7	9.30	27.6
Sr	439	323	283	503	314	220	591	237	430	301	259	519	251	278
V	268	145	224	336	241	184	76.2	222	129	189	196	53.2	23.6	47.2
Y	20.6	30.8	22.1	20.1	26.6	20.9	22.8	31.1	21.3	23.5	21.2	22.7	23.5	18.4
Zn	49.1	96.9	38.4	79.5	85.2	46.3	22.7	55.6	70.2	53.0	49.8	14.5	5.2	40.6
Zr	203	287	171	131	161	154	854	862	628	594	481	1060	964	1020
Cs	<0.4	<0.4	<0.4	19.0	2.83	12.0	<0.4	8.28	15.6	9.34	10.3	12.0	<0.4	13.7
Ge	N.A	N.A	N.A	N.A	N.A	2.1	N.A	N.A	N.A	N.A	N.A	2.3	<2	N.A
Be	4.2	1.8	2.8	2.8	2.5	3.6	5.7	8.1	6.0	16.3	11.4	6.1	1.4	44.9
Nb	15.6	17.3	10.2	3.85	8.03	10.6	24.5	44.0	26.3	38.1	29.8	32.9	28.7	53.0
La	81.0	105	56.4	30.4	55.9	54.7	151	161	101	102	83.3	139	96.4	120
Ce	151	221	121	68.1	116	106	288	349	218	207	173	280	217	267
Pr	19.3	25.7	13.9	8.04	13.0	12.2	34.6	38.4	24.4	24.3	20.6	32.1	24.1	29.1
Nd	74.7	98.1	56.3	30.6	49.5	45.4	127	132	93.3	94.7	80.3	103	79.9	104
Sm	14.4	16.4	9.38	6.27	9.22	8.88	19.2	18.1	15.0	15.2	13.7	16.3	12.0	15.9
Eu	2.88	3.30	2.11	1.57	1.99	1.95	2.75	2.65	2.36	2.66	2.20	2.63	2.12	2.52
Gd	9.39	9.93	5.77	4.63	6.58	6.23	10.1	9.16	7.39	8.65	7.63	8.03	6.35	7.21
Tb	1.20	1.30	0.715	0.624	0.909	0.888	1.28	1.11	0.838	1.03	0.983	0.993	0.735	0.851
Dy	5.78	6.33	3.65	3.38	4.83	4.79	6.27	5.03	3.67	4.99	4.53	4.99	3.94	3.75
Ho	1.05	1.13	0.618	0.612	0.913	0.890	1.11	0.945	0.668	0.894	0.807	0.929	0.728	0.674
Er	2.51	2.70	1.49	1.51	2.32	2.11	2.93	2.59	1.74	2.37	2.16	2.19	1.86	1.83
Tm	0.360	0.374	0.206	0.203	0.319	0.292	0.431	0.362	0.248	0.309	0.275	0.325	0.290	0.242
Yb	2.15	2.32	1.19	1.24	2.05	1.84	2.71	2.18	1.45	1.75	1.80	2.02	1.95	1.49
Lu	0.334	0.311	0.173	0.187	0.309	0.258	0.452	0.324	0.235	0.290	0.266	0.276	0.268	0.234
Hf	6.70	6.92	3.23	2.32	3.90	3.95	29.0	20.7	15.2	17.1	13.6	22.7	17.1	28.4
Ta	0.691	0.911	0.445	0.183	0.388	0.561	2.83	2.70	2.29	3.16	2.28	3.31	2.30	4.92
W	1.74	1.53	0.82	0.25	0.54	0.39	0.57	4.85	0.86	4.22	3.43	0.32	0.31	3.08
Bi	<0.5	<0.5	<0.5	<0.5	<0.5	<0.5	0.83	<0.2	<0.2	0.52	<0.2	0.54	0.51	0.52
Th	35.7	48.1	24.9	9.45	18.0	17.5	117	68.8	56.4	56.8	43.9	78.1	57.7	94.6
U	5.59	9.93	6.70	3.29	5.09	4.18	17.2	21.8	18.2	15.7	11.8	20.7	19.6	26.2
La_N/Lu_N	25.07	34.90	33.70	16.81	18.70	21.92	34.54	51.37	44.43	36.36	32.37	52.06	37.18	53.01
Sm/La	0.178	0.156	0.166	0.206	0.165	0.162	0.127	0.112	0.149	0.149	0.105	0.117	0.125	0.133
Th/La	0.41	0.458	0.441	0.311	0.322	0.319	0.775	0.427	0.558	0.557	0.527	0.562	0.599	0.788
Mg#	72	27	54	65	62	67	64	52	67	73	74	34	27	56

Group	Kinna volcanic succession group 3								Clast	Storgruvpiken rhyolite				RG-2003
Sample	15BD −1329	15BD −592	BD14 −24	BD14 −80	BD14 −84	17BD −42B	15BD −256B	BD15 −256A	BD15 −163	15BD −178	BD14_20	TG12 −739	TGR_ 445	Cont. crust
SiO_2%	50.6	48.4	48.3	48.4	54.7	47.3	58.5	60.1	68.9	69.0	69.8	69.8	68.8	60.6
Al_2O_3	11.7	13.7	17.2	12.7	16.8	17.4	17.8	17.8	15.7	15.6	15.3	15.8	15.4	15.9
Fe_2O_3	6.08	7.75	4.95	8.20	4.76	5.71	2.01	2.38	2.54	1.95	2.31	2.23	2.60	6.71
TiO_2	0.863	1.10	1.03	1.21	1.07	1.45	0.631	0.616	0.114	0.069	0.092	0.049	0.082	0.72
MgO	9.26	10.9	4.29	8.49	3.21	5.12	0.994	1.13	1.05	0.064	0.725	0.649	0.686	4.66
CaO	10.7	6.07	6.54	6.41	3.84	7.82	3.61	2.95	0.718	0.771	0.091	0.145	0.334	6.41
Na_2O	1.55	1.46	1.88	1.53	3.57	1.67	3.52	4.49	6.68	6.18	6.18	4.36	4.30	3.07
K_2O	2.99	5.75	7.93	5.79	7.07	5.94	8.16	6.24	2.91	4.03	3.69	5.05	5.36	1.81
MnO	0.115	0.110	0.092	0.172	0.086	0.083	0.033	0.034	0.028	0.097	0.024	0.024	0.03	0.10
P_2O_5	0.436	0.858	0.723	1.15	0.720	0.606	0.374	0.382	0.076	0.029	0.020	0.020	0.010	0.13
LOI	3.58	1.76	4.22	4.38	1.76	5.09	2.64	2.41	1.02	1.26	0.42	0.96	0.75	
Ba ppm	2650	1700	3070	473	2250	3970	2160	1360	671	179	240	157	374	456
Co	29.0	37.9	22.9	38.0	15.9	27.8	5.3	5.4	<4	<4	<4	<4	<4	26.6
Cr	627	761	51.7	610	36.9	43.3	87.0	70.3	99.5	40.6	32.1	<5	9.6	135
Cu	93.3	<5	543	<5	218	371	8.0	5.7	10.9	<5	<5	21.2	31.2	27
Ga	16.6	15.4	17.6	15.5	13.7	22.7	12.8	13.6	14.4	20.7	20.9	26.5	32.4	16
Ni	250	294	49.7	221	32.6	40.8	13.8	16.9	17.5	<5	<5	4.5	7.2	59
Pb	49.7	55.1	130	56.4	77.7	299	165	111	88.8	30.4	58.4	64.0	79.6	11
Rb	114	386	366	574	352	205	187	172	122	192	242	280	190	49
Sc	22.7	23.2	15.6	24.7	11.2	24.4	13.9	15.1	<5	<5	<5	<5	<5	21.9
Sn	16.7	19.3	21.1	12.4	11.3	18.4	25.5	23.1	13.9	21.7	10.8	18.0	31.6	1.7
Sr	455	207	854	314	592	376	532	403	108	62.3	127	41.2	87.6	320
V	206	165	198	196	127	220	50.5	62.3	36.0	<5	<5	<5	<5	138
Y	21.0	35.7	20.8	17.0	22.6	35.5	27.6	29.4	24.7	63.5	41.4	28.3	67.0	19
Zn	42.7	62.8	31.9	86.7	42.2	33.1	35.9	42.2	13.5	22.3	73.9	62.0	96.0	72
Zr	410	615	659	559	518	778	1130	956	482	530	393	329	525	132
Cs	<0.4	31.0	16.0	54.0	27.0	6.56	<0.4	<0.4	<0.4	<0.4	13.0	<0.4	<0.4	2
Ge	N.A	N.A	17.6	18.1	13.3	N.A	<0.2	2.2	<0.2	<0.2	<0.2	1.1	<0.2	1.3
Be	19.0	15.0	14.8	27.2	60.1	12.7	7.1	8.8	9.0	29.6	6.7	66.5	10.3	1.9
Nb	24.4	41.1	52.9	40.2	40.3	59.0	58.5	48.9	19.6	158	94.8	81.4	176	8
La	78.9	121	110	79.1	84.4	113	110	76.4	58.1	126	39.8	29.6	66.8	20
Ce	179	224	221	188	171	245	228	175	108	273	126	85.8	185	43
Pr	23.0	34.6	27.9	27.7	22.2	30.6	30.4	21.7	14.5	34.1	15.1	9.36	20.0	4.9
Nd	92.7	153	122	141	104	128	129	85.4	58.5	120	62.2	35.5	80.8	20
Sm	16.8	28.5	23.2	29.5	19.0	23.3	22.3	16.2	11.8	25.4	13.5	7.36	18.3	3.9
Eu	3.28	4.40	4.00	3.89	2.95	3.68	3.76	2.67	0.552	0.342	0.179	0.135	0.109	1.1
Gd	8.67	14.8	13.5	13.8	9.98	12.1	11.4	7.89	6.49	14.6	8.84	4.63	11.2	3.7
Tb	1.08	1.65	1.72	1.60	1.34	1.47	1.47	0.988	0.893	2.16	1.30	0.731	2.04	0.6
Dy	5.32	7.43	8.60	7.25	6.81	6.64	6.79	4.89	4.75	12.2	6.45	3.74	10.8	3.6
Ho	0.946	1.25	1.47	1.19	1.21	1.14	1.14	0.865	0.921	2.35	1.17	0.689	2.08	0.77
Er	2.31	2.91	3.95	2.87	2.87	2.94	2.76	2.11	2.37	6.33	2.96	1.98	5.04	2.1
Tm	0.325	0.407	0.538	0.394	0.400	0.391	0.403	0.321	0.385	0.970	0.476	0.299	0.747	0.28
Yb	1.89	2.39	3.24	2.30	2.63	2.37	2.69	1.88	2.54	5.86	3.10	1.99	4.25	1.9
Lu	0.259	0.358	0.464	0.319	0.398	0.358	0.413	0.25	0.380	0.769	0.440	0.274	0.637	0.30
Hf	12.1	19.2	23.9	16.6	14.5	21.3	34.7	20.4	22.9	24.7	14.3	11.4	18.1	3.7
Ta	1.79	2.90	3.83	2.21	2.31	3.44	4.83	3.50	3.13	12.7	8.71	6.95	9.59	0.7
W	3.16	2.10	10.5*	13.0*	10.6*	5.08	1.79	1.83	1.07	3.80	1.21	10.1*	23.3*	1.0
Bi	0.78	0.64	2.12	0.68	0.68	3.71	<0.2	<0.2	3.08	<0.2	1.99	1.34	0.586	0.18
Th	53.5	97.8	136	114	87.4	104	192	131	211	278	120	113	152	5.6
U	18.7	19.2	30.2	24.7	21.5	27.9	12.9	16.5	29.4	36.3	23.0	61.8	58.9	1.3
La_N/Lu_N	31.49	34.94	24.51	25.63	21.92	32.63	27.53	31.59	15.80	16.94	9.35	11.17	10.84	6.89
Sm/La	0.213	0.236	0.211	0.373	0.225	0.206	0.203	0.212	0.203	0.202	0.339	0.249	0.274	0.195
Th/La	0.320	0.808	1.236	1.441	1.036	0.920	1.745	1.725	3.632	2.206	3.015	3.818	2.275	0.28
Mg#	75	74	63	67	57	64	50	49	45	7	38	37	34	

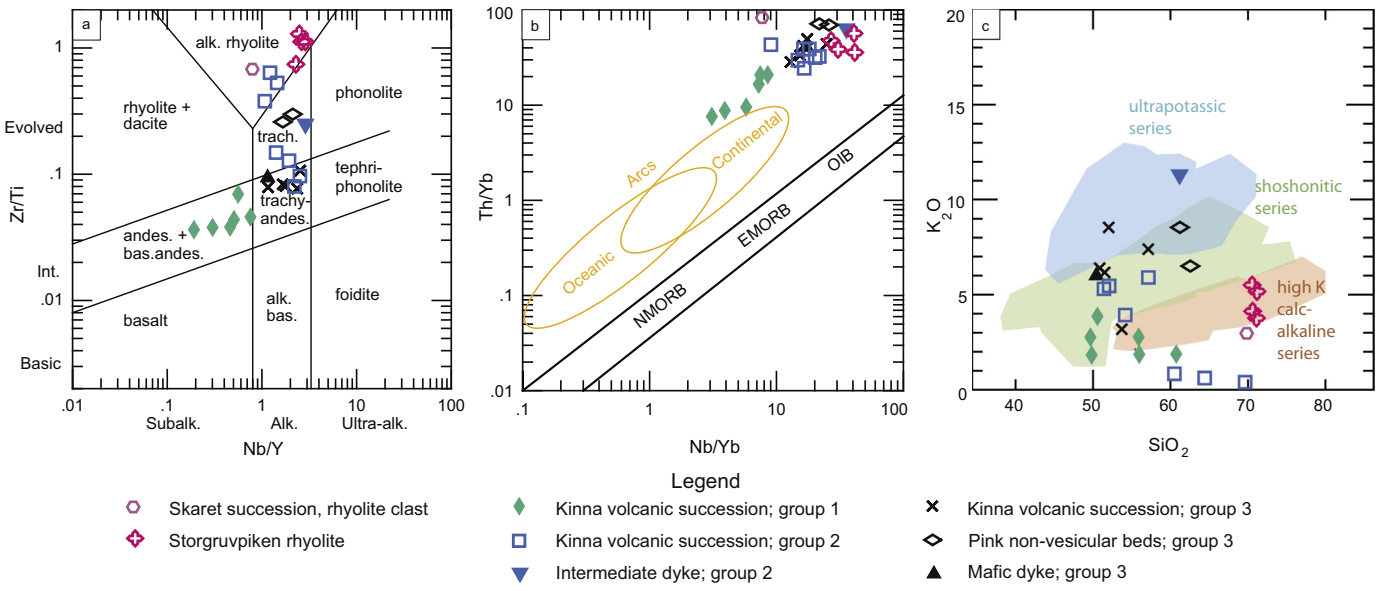

Fig. 7. a. Classification of Skarvatnet unit samples based on the stable elements Zr, Ti, Nb and Y (Pearce, 1996). b Th/Yb vs. Nb/Yb plot (Pearce, 2008) with fields of volcanic rocks from oceanic and continental arcs. All samples from the Skarvatnet unit are highly enriched compared to normal arc rocks. c K_2O vs. SiO_2 plot with fields for high-K calc-alkaline (orange), shoshonitic (green) and ultrapotassic (blue) Italian rocks summarized by Conticelli et al. (2010) for comparison.

According to White (2000), one of the main diagnostic features of submarine pyroclastic flows are enclosing submarine deposits. The Kinna succession interfingers with cherts, siltstones and pillow lavas (Fig. 2), and the associated Skaret succession is clearly shallow-marine. Therefore, we envisage a submarine deposition of the Kinna succession as most likely. However, there is no evidence that the deposits have been sorted by water; the fragments are for instance randomly distributed with respect to fragment size and vesicularity. The regular nature of the beds and the lack of erosional channels or valley fills point to either deposition below wave base or ash fall-outs (Fisher and Schmincke, 1984). However, the lack of sorting within beds is atypical for both subaerial and submarine fallout deposits; poorly sorted, massive but stratified deposits are rather associated with deposition from density currents formed during collapse of subaqueous plumes (Kano, 2003; White, 2000).

Available evidence thus suggests an origin as submarine pyroclastic flows from submarine volcanic eruptions. We envisage a depositional environment around predominantly intermediate to felsic submarine volcanic centres comparable to the recent Myojin Knoll caldera in the Izu-Bonin arc (Fiske et al., 2001), where thick pumice deposits similar to the Kinna fragment-bearing beds are observed. The Kinna volcanic succession also has similarities with the VMS-hosting Bald Mountain, Maine, USA; this deposit consists of beds with pumice and medium- to coarse-grained ash separated by fine-grained tuff beds (Busby, 2005). The pumiceous beds of the Bald Mountain are considered to have formed from an eruption column with limited mixing with ambient water, while the tuff beds represent erupting phases with more admixed water (Busby, 2005; Kessel et al., 2003). Submarine pyroclastic deposits have varying degrees of sorting, depending on size and vesicularity of the fragments, their temperature during eruption and water depth. Products of deep-water eruptions are generally considered to be depleted in fine ash, as a result of either removal of fine ash because of mixing with water (Kano, 2003), or limited fragmentation due to high hydrostatic pressure (Busby, 2005). Unfortunately, the original grain size of the finer material in the Kinna volcanic succession cannot be identified due to metamorphic recrystallization, and can therefore not be used to constrain the depth of water during eruption. However, the Bald Mountain erupted at >1.45 km below sea level (Kessel et al., 2003) and a comparable deep marine setting is possible also for the Kinna volcanic succession.

4.1.2. The Storgruvpiken rhyolite

The Storgruvpiken rhyolite cuts obliquely through the Kinna volcanic succession and has large inclusions of country rock in parts of the body (Fig. 5a), suggesting that it had at least partly an intrusive rather than volcanic origin. The very fine-grained nature is most consistent with a shallow emplacement, and a composite volcanic plug and dome structure is also conceivable. The rhyolite is non-vesicular and almost devoid of hydrous minerals, indicating a volatile-poor magma compared to the Kinna volcanic succession. The high viscosity of such a SiO_2-rich, dry magma would promote the formation of flow-banding, as observed at Storgruvpiken, whether it was in a volcanic dome or in a subvolcanic plug. Phenocrysts of K-feldspar are euhedral, and fragmented phenocrysts are not observed. This indicates that explosive fragmentation was very limited or absent, as phenocrysts are commonly shattered during fragmentation of a magma (e. g. Fisher and Schmincke, 1984).

4.1.3. The Skaret succession

The abundant conglomerates of the Skaret succession, with large blocks and soft-sediment deformation structures in associated sandstones, indicate an origin largely as coarse debris flow deposits. The high diversity of the clast material (basaltic and rhyolitic rocks (Skaret clast; Figs. 7-9), jasper, chert, Kinna-type volcanic clasts, marble, siltstone and sandstone) shows that the source area was complex, but all the material observed could have been derived from local sources within the low-grade metamorphic part of the TNC. The carbonate content of the greywacke, the carbonate clasts and blocks, and presence of carbonate beds show that the sediment was derived from a shallow marine source, and the metre-sized blocks suggest that the source is proximal. The soft-sediment deformation structures, chaotic deposits and large blocks attest to a tectonically active environment and strong relief. There are no direct constraints on the age of the Skaret succession, but conglomerate clasts similar to the Kinna volcanic succession and rhyolite clasts comparable to the Storgruvpiken rhyolite (Skaret clast; Figs. 7-9) indicate that the Skaret succession was deposited after emplacement of the Storgruvpiken rhyolite.

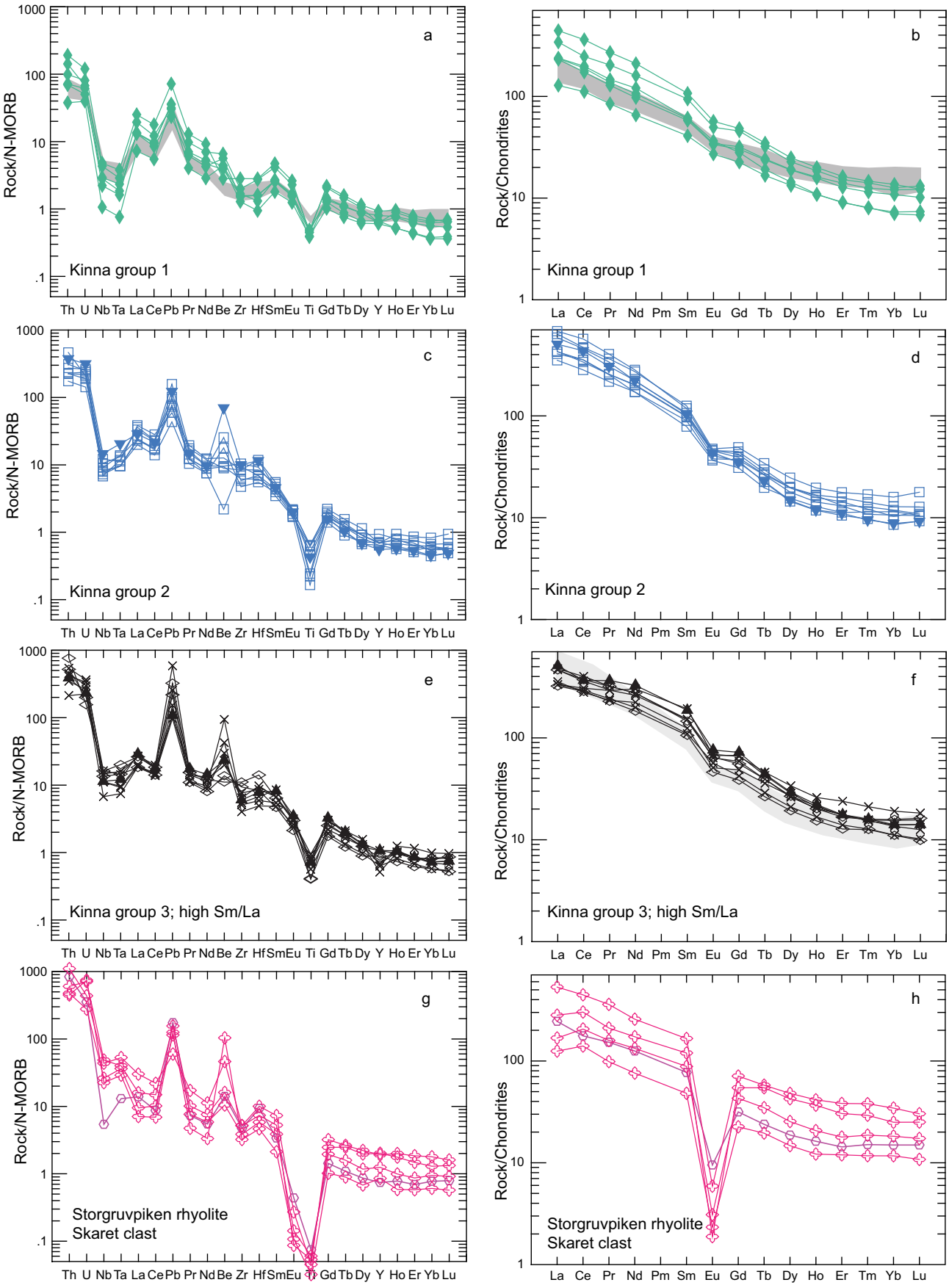

Fig. 8. Left column: Sample versus N-MORB, normalization values from Gale et al. (2013). The position of beryllium is chosen on the basis of its geochemical similarity to Nd and Zr (Ryan, 2002). Right column: Sample versus chondrite, normalization values from Sun and McDonough (1989). The dark grey shaded fields in Fig. 8a and Fig. 8b correspond to the Hølonda porphyrites (Grenne and Roberts, 1998). The light grey shaded field in Fig. 8f corresponds to the REE-patterns of Kinna group 2.

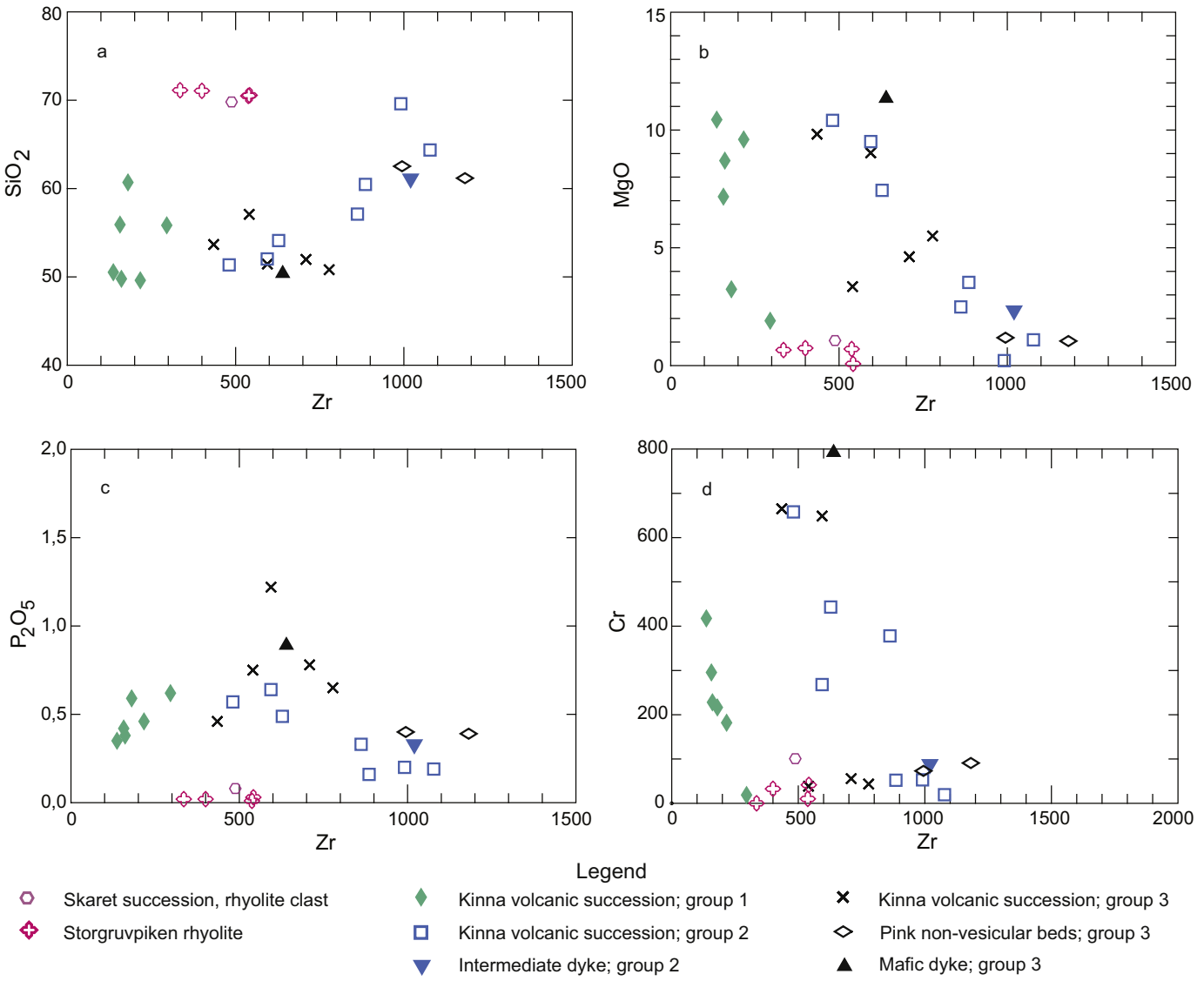

Fig. 9. Zirconium versus SiO_2, MgO, P_2O_5 and Cr. Kinna group 1 and the Storgruvpiken rhyolite plot in separate groups, while there is more overlap between Kinna groups 2 and 3. See text for discussion.

4.2. Petrogenesis

4.2.1. The Kinna volcanic succession

The overall geochemical characteristics of the Kinna volcanic succession, such as Nb, Ta and Ti depletion and Pb enrichment (Fig. 8), show a clear affinity to subduction-related, arc-type rocks. However, compared to more common arc-type rocks, the Kinna rocks are extremely enriched in elements like Th, U, LREE, Be and Zr, they have relatively high K_2O (up to 11 wt%), but also relatively high MgO and Mg#, Cr and Ni (Table 1; Figs. 7–10).

Similar potassic to ultrapotassic, highly enriched volcanic rocks with mantle affinities are rare in modern settings, but the ones that exist have received considerable attention (e.g. Bergman, 1987; Foley, 1992a; Foley et al., 1987; Förster et al., 2017; Prelević et al., 2008; Tommasini et al., 2011). They occur both within plate (anorogenic settings) and along plate boundaries (orogenic or subduction-related settings; e.g. Bergman, 1987; Prelević et al., 2008). Orogenic-type potassic rocks are most common in the Mediterranean and along the Alpine-Himalayan belt, for instance in Spain (e.g. Pérez-Valera et al., 2013), Italy (e.g. Conticelli et al., 2009; Peccerillo, 1999), the Balkan Peninsula (e.g. Prelević et al., 2005), the Aegean (e.g. Ersoy and Palmer, 2013; Pe-Piper et al., 2009), Turkey (Dilek and Altunkaynak, 2009), Iran (e.g. Shafaii Moghadam et al., 2018) and Tibet (e.g. Cheng and Guo, 2017). Plutonic and volcanic rocks with similar geochemical characteristics have also been reported from the older Variscan (e.g. Soder and Romer, 2018) and Caledonian (e.g. Thompson and Fowler, 1986; West et al., 2007) orogenic belts. The striking geochemical similarities noted above lead us to consider these orogenic potassic volcanic rocks the closest analogue for the interpretation of petrogenesis and tectonic setting of the Kinna volcanic succession.

There seems to be a consensus in the literature that the extreme enrichment of various elements in orogenic potassic rocks with obvious mantle signatures (Mg# >70, high MgO, Ni and Cr values) cannot be the result of crustal contamination, assimilation and fractionation of a mantle-derived magma on its way up through the continental crust, but has to be a primary feature of melts derived from anomalously enriched subcontinental lithospheric mantle domains (e.g. Bergman, 1987; Conticelli et al., 2009; Foley et al., 1987; Förster et al., 2017; Prelević et al., 2008; Prelević et al., 2013). Where phenocrysts of olivine, spinel or pyroxene are present, the mineral chemistry (very high Mg#, high Cr and Ni contents) indicate a depleted mantle source for the ultrapotassic rocks (e.g. Förster et al., 2017; Prelević et al., 2013). The

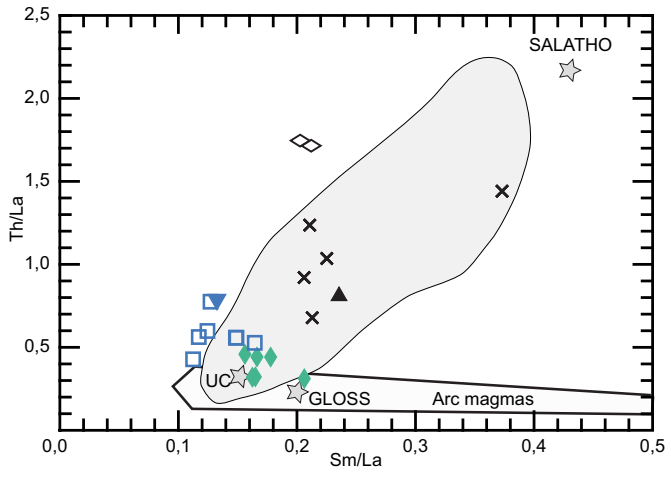

Fig. 10. Th/La versus Sm/La plot for the Kinna volcanic succession. The Storgruvpiken rhyolite samples have extreme Th/La ratios and plot outside the diagram. GLOSS (Global Subducting Sediment; Plank and Langmuir, 1998) and UC (Upper Crust; Rudnick and Gao, 2003) represent average composition of recycled crustal material. The arc magma field is from Plank (2005) and represents 'normal' arc magmas. The grey field represents analyses from Tethyan lamproites and related rocks from Tommasini et al. (2011). SALATHO is the high Sm/La and Th/La component of Tommasini et al. (2011).

whole rock chemistry of several Kinna rocks is comparable to mantle-derived ultrapotassic rocks studied by e.g. Prelević et al. (2013), but the lack of preserved phenocrysts of olivine or pyroxene in the metamorphosed Kinna rocks hampers more detailed interpretations of the mantle source composition for the latter. The crustal-like enrichment signatures of orogenic potassic rocks are generally assigned to a metasomatic agent derived from subducting continental material (e.g. Conticelli et al., 2009; Plank and Langmuir, 1998; Prelević et al., 2013). Transport of incompatible elements from the subducting slab into the overlying mantle wedge is more efficient by partial melts (including supercritical fluids) of slab components, than by aqueous fluids released during dehydration (e.g. Conticelli et al., 2010; Hermann and Rubatto, 2009; Spandler and Pirard, 2013). High-pressure melts of crustal rocks have K/Na molar ratios of 1.4–2 (Schmidt et al., 2004), and the high K_2O of ultrapotassic rocks indicate addition of such crustal components to the mantle (Soder and Romer, 2018).

Partial melting of slab components at sub-arc depths seems to be a common feature in many subduction zones, with the fluids needed for melting derived from dehydration of serpentinites from either the oceanic lithospheric mantle or from within the mélange zone at the top of the down-going slab (e.g. Spandler and Pirard, 2013), or derived from high pressure dehydration of phengite in subducted continental crust or sediments (Hermann and Rubatto, 2009; Schmidt et al., 2004). The trace element budget of these melts is controlled by the stability of accessory phases such as monazite/allanite (LREE, Th, U), phengite (LILE), titanite (REE, Nb, Ta), rutile (Nb, Ta), zircon (Zr, Hf), garnet (HREE), zoisite/epidote (REE, Sr, Th, U, Pb) and lawsonite (REE, Pb, Sr) (Hermann and Rubatto, 2009; Spandler et al., 2003). Breakdown of for example monazite/allanite together with residual garnet and rutile generally explains the enrichment of LREE over HREE as well as the negative Nb—Ta anomalies of typical arc rocks (e.g.; Hermann and Rubatto, 2009).

The trace element patterns and ratios of Kinna rocks (Figs. 8-10) correspond well with an origin from a mantle metasomatized by partial melts of common subducting slab components (i.e. pelitic sediments, continental crust) with the Th and REE element budget controlled by common accessory phases such as monazite/allanite, rutile and garnet (e.g. Figs. 8-10; Spandler and Pirard, 2013). However, the Sm/La vs. Th/La ratios of the Kinna group 3 samples are distinctly different from those of Kinna 1 and 2 and are also different from common arc magmas, falling along a positive trend towards the SALATHO component of Tommasini et al. (2011; Fig. 11). Such a positive trend is present in many lamproites from the Alpine-Himalayan chain (e.g. Tommasini et al., 2011) as well as in Variscan lamprophyres (Soder and Romer, 2018). This relation requires a component that simultaneously fractionates Th—La and Sm—La, and Tommasini et al. (2011) consider blueschist-facies mélanges rich in lawsonite and zoisite-epidote the source for this unusual composition. Such lithologically complex mélange zones, consisting of a mixture of oceanic crust, sediments and mantle wedge/forarc lithologies enable a variety of fluids and melts to be produced during progressive subduction (Bebout and Penniston-Dorland, 2016; Marschall and Schumacher, 2012) and may add considerable compositional complexity to the mantle wedge (e.g. Guo et al., 2014; Prelević et al., 2013; Spandler and Pirard, 2013).

The Kinna 3 melts could therefore have been derived from a mantle domain strongly metasomatized by a mélange-derived agent, in contrast to the Kinna 1 and 2 melts. Alternatively, Soder and Romer (2018) ascribe high Sm/La vs. Th/La ratios of the Variscan lamprophyres

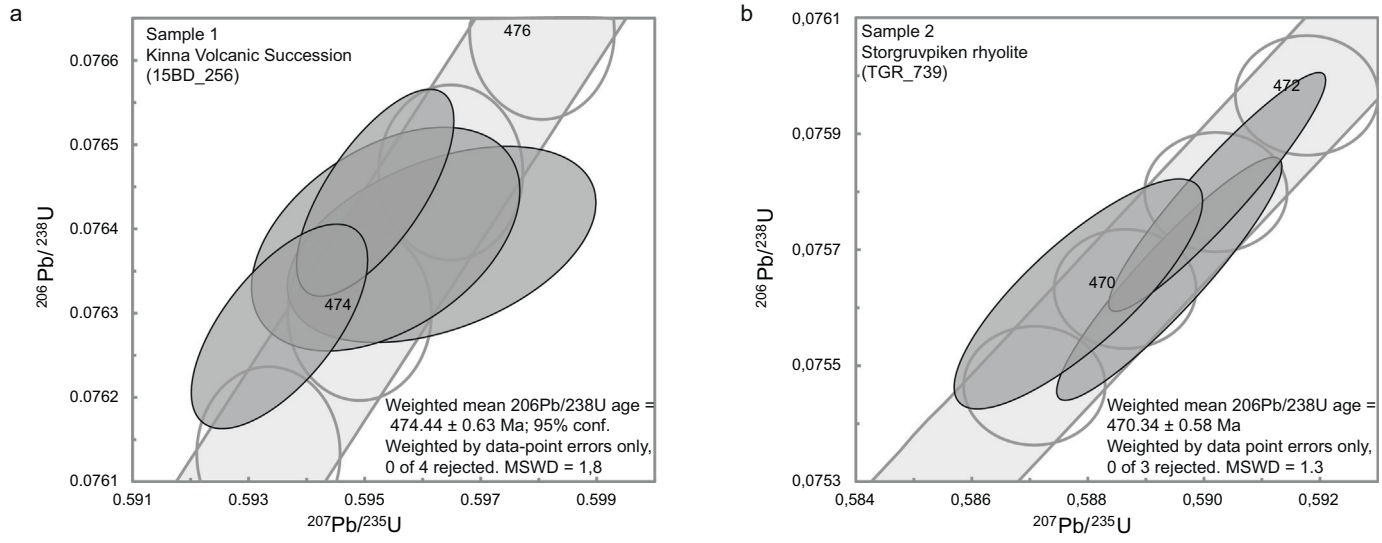

Fig. 11. Concordia plots for the zircon U—Pb TIMS data. Data point ellipses are 2σ; plots are made with ISOPLOT (Ludwig, 2003). a Sample 1: Pink non-vesicular bed from the Kinna volcanic succession, with a mean age of 474 ± 1 Ma (2σ; MSWD = 1.8). b Sample 2: Storgruvpiken rhyolite, with a mean age of 470 ± 1 Ma (2σ; MSWD = 1.3).

Table 2
U—Pb analytical data. a ZR = zircon; lrg = large, fr = fragment, eu = euhedral, eq = equant, br = brown, pnk = pink, AA = air abraded, CA = chemically abraded. b Th/U model ratio inferred from $^{208}Pb/^{206}Pb$ ratio and age of sample. c Pbc = total common Pb (initial + blank). d raw data, corrected for fractionation and spike. e ratio of radiogenic Pb over common Pb (including blank). f corrected for fractionation, spike, blank and initial common Pb (based on Stacey and Kramers, 1975); error calculated by propagating the main sources of uncertainty; The U—Pb ratio of the spike used for this work is adapted to $^{206}Pb/^{238}U = 0.015660$ for the ET100 solution as obtained with the ET2535 spike at NIGL.

						Isotopic ratios							AGE [Ma]					
Sample (a)	U [ppm]	Th/U (b)	Pb_c (pg) (c)	$^{206}Pb/^{204}Pb$ (d)	Pb^*/Pb_c (e)	$^{207}Pb/^{235}U$ (f)	2 sigma % (f)	$^{206}Pb/^{238}U$ (f)	2 sigma % (f)	corr. coef.	$^{207}Pb/^{206}Pb$ (f)	2 sigma % (f)	$^{206}Pb/^{238}U$ (f)	± 2 sigma (f)	$^{207}Pb/^{235}U$ (f)	± 2 sigma (f)	$^{207}Pb/^{206}Pb$ (f)	± 2 sigma (f)
Sample 1, Kinna volcanic succession (15-BD-256A)																		
1 LRG ZR FR CLEAR CA	1670	0.78	1.3	6085	111	0.59518	0.19	0.07644	0.13	0.70	0.05647	0.13	474.9	0.6	472.4	0.7	470.9	3.0
1 ZR FR CLEAR CA	317	0.73	1.2	1249	22	0.59633	0.36	0.07638	0.12	0.43	0.05662	0.33	474.5	0.6	474.9	1.4	476.9	7.3
1 ZR FR CLEAR CA	787	0.71	1.5	2447	44	0.59536	0.32	0.07639	0.14	0.43	0.05653	0.29	474.5	0.6	474.3	1.2	473.1	6.3
1 ZR FR CLEAR CA	1439	0.62	2.5	2738	47	0.59353	0.21	0.07628	0.13	0.65	0.05643	0.16	473.9	0.6	473.1	0.8	469.3	3.5
Sample 2, Storgruvpiken rhyolite (TGR12_739)																		
1 Z EU-EQ. BR AA	5108	0.43	4.2	5755	189	0.58940	0.27	0.07565	0.23	0.92	0.05651	0.11	470.1	1.0	470.5	1.0	472.4	2.3
1 Z EQ-EU BR AA	3576	0.41	1.1	15,947	353	0.59023	0.26	0.07580	0.22	0.94	0.05647	0.09	471.0	1.0	471.0	1.0	471.1	2.0
1 Z EU-EQ PNK AA	2047	0.45	2.7	3579	229	0.58784	0.30	0.07562	0.21	0.81	0.05638	0.18	469.9	1.0	469.5	1.1	467.2	3.9

to the presence of residual allanite in partial melts derived from crustal material under high pressure conditions. A similar origin for the Kinna volcanic succession can be envisaged: Kinna 1 and 2 could be derived from mantle domains that were metasomatized by an agent where allanite was dissolved into the melt, whereas Kinna 3 could be derived from mantle domains metasomatized by an agent where allanite was a residual phase during formation of the agent by partial melting of continental material. Soder and Romer's (2018) explanation of high Sm/La vs. Th/La ratios is more straightforward than the model of Tommasini et al. (2011) and does not require a totally different origin of the metasomatic melts (continental material versus blueschist melange), but only requires variable allanite dissolution into a metasomatic agent derived from subducted continental material. The steep slope of the Kinna REE patterns, with strong LREE enrichment (Fig. 8) might indicate the presence of garnet in the source, either in the subducted continent-derived material or in the metasomatically altered mantle, since garnet easily accommodates HREE but not LREE (e.g. Hermann and Rubatto, 2009).

Mantle metasomatism is generally assumed to occur within localized networks of veins and fractures, leading to mantle domains with phlogopite-, amphibole- and/or pyroxene-rich veins and dykes within peridotitic wall-rocks (e.g. Foley, 1992a; Foley, 1992b; Förster et al., 2017; Marocchi et al., 2010; Spandler and Pirard, 2013). Transitions from high-K through shoshonitic to ultrapotassic rocks are generally explained by processes where partial melts received variable contributions from either vein or wall-rock domains (e.g. Conticelli et al., 2010; Förster et al., 2017; Marocchi et al., 2010). We therefore envisage that the variation from high-K to ultrapotassic rocks observed within the Kinna volcanic succession (Fig. 7c), at least partly could be the result of variable vein/wall-rock contribution during mantle partial melting.

4.2.2. The Storgruvpiken rhyolite

The Storgruvpiken rhyolite is apparently unique in the Scandinavian Caledonides; to our knowledge no other rhyolite in this part of the orogen is similarly enriched in e.g. Be and Th. On the other hand it shares several geochemical features with the older Kinna volcanic succession, including high Th, Zr and Be concentrations and LREE enrichment, potentially indicating that they might have a related origin by, for example, differentiation and fractional crystallisation processes. However, the ca. 4 m.y. difference in age and key geochemical characteristics listed in the following suggest that this is not the case.

Compared to the Kinna 1 samples, the rhyolites have higher Zr (Fig. 9) that could be interpreted in terms of fractional crystallisation, but such a relationship conflicts with their significantly different ratios of highly incompatible trace elements, e.g., Th/La and Ta/La ratios (Fig. 8). Compared to the Kinna 2 samples, the Storgruvpiken rocks have low Zr concentrations that possibly could be interpreted in terms of crystallisation and removal of zircon from strongly fractionated melts; however, again this conflicts with the significantly different trace elements patterns (Fig. 8). Moreover, the lack of a compositional continuum from Kinna rocks to the voluminous Storgruvpiken rhyolite (Fig. 9) is noteworthy and argues against a fractional crystallisation connection. Furthermore, the rhyolites have peraluminous and A-type characteristics, which are commonly associated with partial melting of crustal rocks (Barbarin, 1999) rather than mantle derivation, different from those of Kinna. Therefore, an origin of the Storgruvpiken rhyolite as a differentiation product of one of the Kinna types is ruled out.

Alternatively, The Storgruvpiken rhyolite could have a similar veined mantle source as the Kinna rocks, with a different vein/wall-rock contribution during partial melting. However, the Storgruvpiken rhyolite has a highly evolved chemical composition that requires extensive fractionation from a larger volume of mantle melt. The large volume of the Storgruvpiken rhyolite and the lack of a mafic or intermediate counterpart argue against this explanation.

Another model for the Storgruvpiken rhyolite might involve partial melts of subducted material that rose diapirically directly through the mantle instead of reacting metasomatically with it. Such diapiric rise of subducted mélange material has been suggested by Marschall and Schumacher (2012). Their model suggests that heating from the surrounding mantle and consequent dehydration of such diapirs initially leads to hydrous mantle melting, which produces melts enriched in fluid-mobile elements. Further heating of the rising diapir produces dry magmas with higher contents of immobile elements like Th and Be. In this line of reasoning, Kinna 1 could result from melting of a hydrated mantle and the Storgruvpiken rhyolite could represent late stage dry melting of such a diapir; however, this model does not explain the strong enrichment of immobile elements in the clearly mantle-derived Kinna rocks.

It is also possible that the Storgruvpiken rhyolite genesis involved magmas similar to the Kinna volcanic succession, derived by partial melting of metasomatized mantle and with high Th, LREE, HFSE etc., that crystallized at depth in the crust or at the crust-mantle interface. Subsequent partial melting of such enriched rocks under lower crustal conditions may produce felsic magma and is likely to leave plagioclase and amphibole as residual phases (Qian and Hermann, 2013). With the mineral/melt partition coefficients given by Qian and Hermann (2013), residual plagioclase is consistent with the negative Eu anomaly as well as the higher Th/La and Nb/La of the Storgruvpiken rhyolite compared to the Kinna volcanic succession. Partial melting in the lower crust also allows for melting of some metasedimentary rocks and reaction between melts, possibly accounting for the peraluminous character of the Storgruvpiken rhyolite. In view of the absence of other than strongly

enriched rocks in the area, this scenario requires that remelting of Kinna-type intrusions was more significant than melting of surrounding 'normal' lower crust at least on a local scale. Given the relatively short time span between the dated part of the Kinna volcanic succession and the Storgruvpiken rhyolite (<4 Ma), it is reasonable to assume that the Kinna-type intrusions remained hotter than the surrounding lower crust. Together with a higher content of hydrous minerals (biotite, amphibole), which are common constituents of the Kinna volcanic succession, this would have made the intrusions more susceptible to melting compared to normal lower crust (Annen and Sparks, 2002).

4.2.3. Beryllium enrichments

A peculiar feature of the Storgruvpiken rhyolite, partly also of the Kinna volcanic rocks, is the very strong enrichment in beryllium (up to 66.5 ppm Be; Table 1). For comparison, the Miocene Spor Mountain rhyolites in western Utah, USA, which host the world's largest beryllium deposit, contain up to 75 ppm Be in matrix glass (Dailey et al., 2018). Economic concentrations of bertrandite in adjacent tuffs at Spor Mountain (up to 0.3 wt% Be), may have been facilitated by fluids released from the rhyolite lava during crystallisation or devitrification (Christiansen et al., 1986). Although the Kinna pyroclastic volcanic rocks potentially could have served as a comparable host for Be enrichment from Storgruvpiken-derived fluids, economic-grade Be concentrations remain to be found; the highest value detected in the present study within the Kinna succession is 60.1 ppm Be (Table 1).

Arc magmas generally have higher concentrations of Be compared to MORB; reflecting the mobility of Be from the sedimentary cover of subducted crust to the mantle at high P and T (Marschall et al., 2007). Beryllium is generally thought to be immobile during dehydration; however, only a small amount of Be added to the mantle wedge can be sufficient to produce the enrichment observed in arc rocks (Marschall et al., 2007). Ryan (2002) found that more Be is transferred from the subducted slab to the overlying mantle with increasing pressure and temperature and that Be contents are generally higher in alkaline rocks. Partition coefficient data for Be are scarce, but Be is known to be accommodated in biotite, plagioclase and K-feldspar in peraluminous silica-rich systems (Bea et al., 1994). Hence Be enrichments may be explained by small amounts of partial melting of crustal rocks, leading to break-down of biotite in the source rock, as inferred for the Be—Th rich A-type rhyolites at Spor Mountain (Christiansen et al., 1988) which show several geochemical similarities with the Storgruvpiken rhyolite. The Be-enrichment of the Storgruvpiken rhyolite is therefore interpreted as a result of partial melting of biotite-bearing Kinna-type rocks at crustal depth.

4.3. Tectonic model and regional geological implications

Our new data indicate that high-K to ultrapotassic mantle-derived volcanism occurred at 475–470 Ma in terranes now represented in the TNC, post-dating formation of the supra-subduction zone LVB ophiolites of the northwestern TNC. The timing of this volcanism corresponds with obduction of the LVB ophiolites onto a continental margin, supposedly on the Laurentian side of Iapetus, and we infer a link between the obduction and the onset of the potassic mantle-derived volcanism. Based on these temporal relationships we propose the following three-stage model for the tectonic evolution of the Kinna volcanic succession and associated rocks:

(1) A southeast-dipping intra-oceanic subduction zone produced an oceanic island arc with associated back-arc basin (the LVB ophiolites) at 487 to 480 Ma (Fig. 12a) (e.g. Slagstad et al., 2014).
(2) At ca. 480 Ma, the Laurentian margin or a related microcontinent arrived at this subduction zone, leading to an increased input of terrigenous sediments and possibly crustal slivers into the subduction zone (Fig. 12b). Partial melts derived from these crustal rocks affected the overlying mantle wedge, producing a network of metasomatic veins surrounded by unaltered mantle wall rock. In order to produce Kinna 1 and 2 metasomatic agents, extensive breakdown of allanite must have occurred during melting of the crustal rocks, whereas the Kinna 3 metamorphic agent with high Sm/La and Th/La ratios might be derived from melts where allanite remained as a residual phase (e.g. Soder and Romer, 2018).
(3) Ongoing convergence led to obduction of parts of the LVB island arc, as well as formation of a thrust stack in the underlying continental margin, which resisted subduction due to buoyancy. This may have resulted in slab retreat and finally break-off of the downgoing oceanic slab, where asthenospheric upwelling might have provided the heat for partial melting of previously metasomatized mantle lithologies (Fig. 12c). Some of these partial melts rose directly to the surface, producing the hydrous melts and explosive volcanism of Kinna 1, 2 and 3 type at ca. 474 Ma. Other melt batches may have crystallized as Kinna-type plutons at depth in the crust and were later possibly partially remelted to produce the dry melts of the Storgruvpiken rhyolite at ca. 470 Ma.

This interpretation infers that the Kinna and Storgruvpiken volcanic rocks were not simply related to normal subduction-related arc

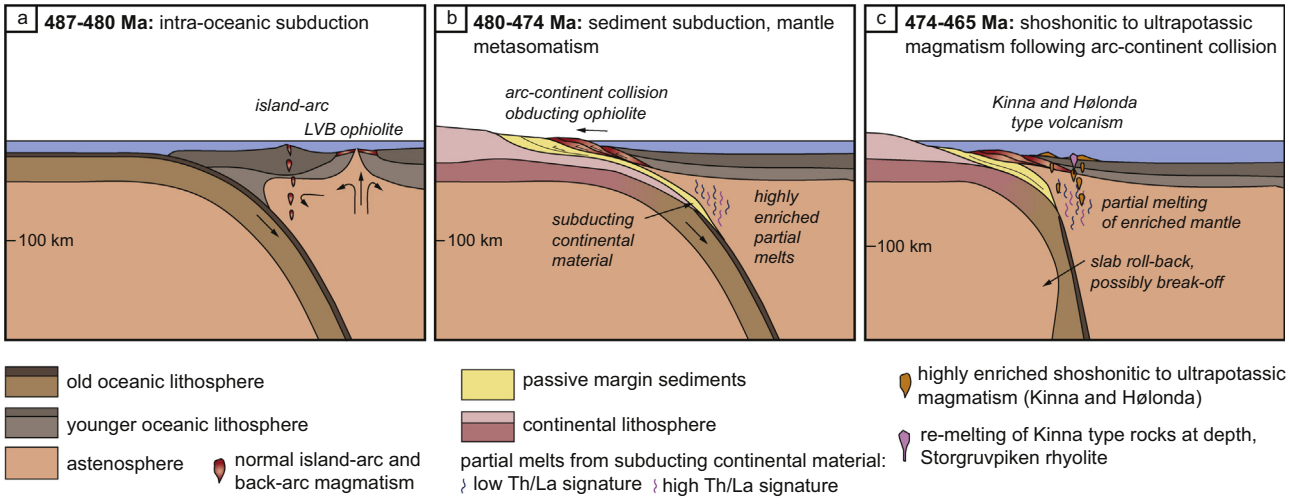

Fig. 12. Tectonic model for the formation of the Skarvatnet unit. See text for discussion.

magmatism, but instead represent the remnants of a distinct tectonic phase along the Laurentian margin of Iapetus, subsequent to the intra-oceanic subduction that dominated the early stages of Iapetus closure. The intra-oceanic subduction terminated when it encountered the Laurentian margin, and slab break-off or other processes led to an intermittent phase producing the highly enriched high-K to ultrapotassic magmatism in the Skarvatnet unit. Such an intermittent tectonic phase has not yet been recognized along the Iapetus margin elsewhere, but the similarly aged Taconian orogen in the Appalachians might have experienced a comparable evolution. There, the Laurentian margin was thrusted under the Notre Dame Arc and equivalents in the Early Ordovician, leading to slab break-off followed by subduction polarity flip and accretion of several ophiolites and arc fragments (e. g. Lissenberg et al., 2005). Although shoshonitic and related potassic rocks are rare in the Appalachians, a 464–462 Ma monzogabbro within the Annieopsquotch Accretionary Tract has shoshonitic geochemical characteristics (Lissenberg et al., 2005) and could be the result of a process similar to that of the Kinna volcanic succession. Slab roll-back (e.g. Cheng and Guo, 2017; Conticelli et al., 2009; Guo et al., 2014) and slab break-off (e.g. Pe-Piper et al., 2009) are also considered as triggering factors for partial melting of metasomatized mantle domains for parts of the Alpine-Himalayan ultrapotassic rocks.

As a consequence of this interpretation, also the tectonic significance of the Hølonda porphyrites has to be reconsidered. These rocks, like the Kinna 1 volcanic rocks, are shoshonitic and are significantly enriched in LREEs and Th (Grenne and Roberts, 1998) although with less extreme compositions (Fig. 8a, b). Many of the Mediterranean potassic to ultrapotassic mantle-derived rocks are associated with less-enriched calc-alkaline to shoshonitic rocks, interpreted to represent partial melts of less-metasomatized mantle domains or larger amounts of wall-rock versus vein-derived mantle melts (e.g. Conticelli et al., 2009; Conticelli et al., 2010; Peccerillo and Martinotti, 2006). Based on the interpretation of these Mediterranean examples of calc-alkaline to ultrapotassic rock suites, we propose that also the Kinna and Hølonda volcanic rocks are related, and that they resulted from the same process of partial melting of variably enriched mantle after arc-continent collision (Fig. 12c). This is at variance with the existing model where the Hølonda porphyrites reflect the first proper subduction below the Laurentian margin, a model that would require very quick polarity flip after obduction of the LVB ophiolite (Grenne and Roberts, 1998). Such a quick subduction polarity flip is not required in our present model, which opens for the possibility that, in this part of the orogen, subduction below the Laurentian margin did not start until ca. 460 Ma, as represented for example by much less enriched arc-type plutons e.g. in the Smøla-Hitra region (Tucker et al., 2004).

5. Conclusions

The Skarvatnet unit, consisting of the Kinna volcanic succession, the Storgruvpiken rhyolite and the Skaret sedimentary succession, represents a lithologically and geochemically distinctive volcano-sedimentary phase hitherto unknown in the Ordovician of the Scandinavian Caledonides. The Kinna volcanic succession is interpreted as a series of submarine pyroclastic flows extruding at ca. 474 Ma, which were intruded by the subvolcanic Storgruvpiken rhyolite at ca. 470 Ma and were subsequently overlain by the shallow-marine Skaret succession in a tectonically active setting. The Kinna volcanic succession shows geochemical signatures far more enriched in for instance Th, U, Pb and LREE than common arc-related rocks, similar to high-K to ultrapotassic rocks of the Alpine-Himalayan belt and other orogenic settings. Based on the comparison with these better studied rock suites, the Kinna volcanic succession is interpreted as representing partial melts derived from previously enriched mantle sources. Enrichment of the mantle source is related to subduction of large amounts of continent-derived material, releasing highly enriched partial melts interacting with the overlying mantle. In the case of the Kinna volcanic succession, this mantle enrichment might have occurred during initial subduction of the Laurentian margin or an associated micro-continent below the originally intra-oceanic LVB arc. Partial melting of the enriched mantle occurred coeval with or slightly after arc-continent collision, possibly facilitated by astenospheric upwelling related to slab retreat or break-off. The Storgruvpiken rhyolite is possibly the result of remelting of Kinna-type plutonic rocks at depth, caused by the same upwelling at ca. 470 Ma.

The slightly younger shoshonitic Hølonda porphyrites are interpreted to be a part of this tectono-magmatic phase, in contrast to earlier interpretations that postulate the Hølonda magmas as a result of subduction below Laurentia subsequent to slab polarity reversal. The existence of extremely enriched volcanic rocks of this type long before the final closure of the Iapetus Ocean demonstrates that such rocks may form not only during or after major continent-continent collisions, but also during earlier phases in complex subduction–accretion–collision systems.

Acknowledgements

E. W. Stokke assisted in the field and lab, G. Fjeld Bye and the technical staff at NGU has prepared and/or analysed samples. Discussions with A. Andresen, J. P. Nystuen and T. Andersen are highly appreciated. Editorial handling by Michael Roden and constructive feedback from reviewers Christian Soder and Dejan Prelević helped to improve the manuscript.

Funding

This work is a part of the first authors PhD thesis, funded by the University of Oslo. The Geological Survey of Norway has funded fieldwork and geochemical analyses under project number 353000.

Declaration of Competing Interests

The authors declare that they have no known competing financial interests or personal relationships that could have appeared to influence the work reported in this paper.

References

Annen, C., Sparks, R., 2002. Effects of repetitive emplacement of basaltic intrusions on thermal evolution and melt generation in the crust. Earth Planet. Sci. Lett. 203, 937–955.
Augland, L.E., Andresen, A., Corfu, F., 2010. Age, structural setting, and exhumation of the Liverpool Land eclogite terrane, East Greenland Caledonides. Lithosphere 2, 267–286.
Barbarin, B., 1999. A review of the relationships between granitoid types, their origins and their geodynamic environments. Lithos 46, 605–626.
Bea, F., Pereira, M., Stroh, A., 1994. Mineral/leucosome trace-element partitioning in a peraluminous migmatite (a laser ablation-ICP-MS study). Chem. Geol. 117, 291–312.
Bebout, G.E., Penniston-Dorland, S.C., 2016. Fluid and mass transfer at subduction interfaces—the field metamorphic record. Lithos 240, 228–258.
Bergman, S.C., 1987. Lamproites and other potassium-rich igneous rocks: a review of their occurrence, mineralogy and geochemistry. Geol. Soc. Lond. Spec. Publ. 30, 103–190.
Bowring, J.F., McLean, N.M., Bowring, S., 2011. Engineering cyber infrastructure for U-Pb geochronology: Tripoli and U-Pb_Redux. Geochem. Geophys. Geosyst. 12 (no. 6).
Bruton, D.L., Bockelie, J.F., 1980. Geology and paleontology of the Hølonda area, western Norway—a fragment of North America. The Caledonides in the USA. Virginia Polytechnic Institute and State University, Department of Geological Sciences. Memoir 2, 41–47.
Busby, C., 2005. Possible distinguishing characteristics of very deepwater explosive and effusive silicic volcanism. Geology 33, 845–848.
Cheng, Z., Guo, Z., 2017. Post-collisional ultrapotassic rocks and mantle xenoliths in the Sailipu volcanic field of Lhasa terrane, South Tibet: Petrological and geochemical constraints on mantle source and geodynamic setting. Gondwana Res. 46, 17–42.
Christiansen, E.H., Burt, D.M., Sheridan, M.F., 1986. The geology and geochemistry of Cenozoic topaz rhyolites from the western United States. Geol. Soc. Am. Spec. Pap. 205.
Christiansen, E.H., Stuckless, J.S., Funkhouser, M., Howell, K., 1988. Petrogenesis of rare-metal granites from depleted crustal sources: an example from the Cenozoic of western Utah, USA. Recent advances in the Geology of Granite-Related Mineral Deposits. Canadian Institute of. Min. Metall. 39, 307–321.
Conticelli, S., Guarnieri, L., Farinelli, A., Mattei, M., Avanzinelli, R., Bianchini, G., Boari, E., Tommasini, S., Tiepolo, M., Prelević, D., 2009. Trace elements and Sr–Nd–Pb isotopes of K-rich, shoshonitic, and calc-alkaline magmatism of the Western Mediterranean Region: genesis of ultrapotassic to calc-alkaline magmatic associations in a post-collisional geodynamic setting. Lithos 107, 68–92.
Conticelli, S., Laurenzi, M.A., Giordano, G., Mattei, M., Avanzinelli, R., Melluso, L., Tommasini, S., Boari, E., Cifelli, F., Perini, G., 2010. Leucite-bearing (kamafugitic/leucititic) and-free (lamproitic) ultrapotassic rocks and associated shoshonites from Italy: constraints on petrogenesis and geodynamics. J. Virtual Explor. 36 (20).

Corfu, F., Andersen, T., Gasser, D., 2014. The Scandinavian Caledonides: main features, conceptual advances and critical questions. Geol. Soc. Lond. Spec. Publ. 390, 9–43.

Dailey, S.R., Christiansen, E.H., Dorais, M.J., Kowallis, B.J., Fernandez, D.P., Johnson, D.M., 2018. Origin of the fluorine-and beryllium-rich rhyolites of the Spor Mountain Formation, Western Utah. Am. Mineralogist: J. Earth and Planetary Mater. 103, 1228–1252.

Dilek, Y., Altunkaynak, Ş., 2009. Geochemical and temporal evolution of Cenozoic magmatism in western Turkey: mantle response to collision, slab break-off, and lithospheric tearing in an orogenic belt. Geol. Soc. Lond. Spec. Publ. 311, 213–233.

Ersoy, E.Y., Palmer, M.R., 2013. Eocene-Quaternary magmatic activity in the Aegean: implications for mantle metasomatism and magma genesis in an evolving orogeny. Lithos 180, 5–24.

Fisher, R.V., Schmincke, H.-U., 1984. Pyroclastic Rocks (Springer Science & Business Media).

Fiske, R.S., Naka, J., Iizasa, K., Yuasa, M., Klaus, A., 2001. Submarine silicic caldera at the front of the Izu-Bonin arc, Japan: Voluminous seafloor eruptions of rhyolite pumice. Geol. Soc. Am. Bull. 113, 813–824.

Foley, S., 1992a. Petrological characterization of the source components of potassic magmas: geochemical and experimental constraints. Lithos 28, 187–204.

Foley, S., 1992b. Vein-plus-wall-rock melting mechanisms in the lithosphere and the origin of potassic alkaline magmas. Lithos 28, 435–453.

Foley, S., Venturelli, G., Green, D., Toscani, L., 1987. The ultrapotassic rocks: characteristics, classification, and constraints for petrogenetic models. Earth Sci. Rev. 24, 81–134.

Förster, M.W., Prelević, D., Schmück, H.R., Buhre, S., Veter, M., Mertz-Kraus, R., Foley, S.F., Jacob, D.E., 2017. Melting and dynamic metasomatism of mixed harzburgite+ glimmerite mantle source: Implications for the genesis of orogenic potassic magmas. Chem. Geol. 455, 182–191.

Gale, A., Dalton, C.A., Langmuir, C.H., Su, Y., Schilling, J.G., 2013. The mean composition of ocean ridge basalts. Geochem. Geophys. Geosyst. 14, 489–518.

Gee, D., Guezou, J., Roberts, D., Wolff, F., 1985. The central-southern part of the Scandinavian Caledonides. The Caledonide orogen-Scandinavia and related areas 1, 109–133.

Grenne, T., Roberts, D., 1998. The Hølonda Porphyrites, Norwegian Caledonides: geochemistry and tectonic setting of Early–Mid-Ordovician shoshonitic volcanism. J. Geol. Soc. Lond. 155, 131–142.

Grenne, T., Ihlen, P., Vokes, F., 1999. Scandinavian Caledonide metallogeny in a plate tectonic perspective. Mineral. Deposita 34 (5–6), 422–471.

Guo, Z., Wilson, M., Zhang, L., Zhang, M., Cheng, Z., Liu, J., 2014. The role of subduction channel mélanges and convergent subduction systems in the petrogenesis of post-collisional K-rich mafic magmatism in NW Tibet. Lithos 198, 184–201.

Hastie, A.R., Kerr, A.C., Pearce, J.A., Mitchell, S., 2007. Classification of altered volcanic island arc rocks using immobile trace elements: development of the Th–Co discrimination diagram. J. Petrol. 48, 2341–2357.

Hermann, J., Rubatto, D., 2009. Accessory phase control on the trace element signature of sediment melts in subduction zones. Chem. Geol. 265, 512–526.

Jaffey, A., Flynn, K., Glendenin, L., Bentley, W.t., Essling, A., 1971. Precision measurement of half-lives and specific activities of U 235 and U 238. Phys. Rev. C 4, 1889–1906.

Kano, K., 2003. Subaqueous pumice eruptions and their products: a review. Washington DC American Geophysical Union Geophysical Monograph Series 140, 213–229.

Kessel, L.G., Busby, C.J., White, J., Smellie, J., Clague, D., 2003. Analysis of VHMS-hosting ignimbrites erupted at bathyal water depths (Ordovican Bald Mountain sequence, northern Maine). Geophys. Monograph Am. Geophys. Union 140, 361–379.

Krill, A.G., 1980. Tectonics of the Oppdal area, Central Norway. Geologiska Föreningen i Stockholm Förhandlingar 102, 523–530.

Krogh, T., 1973. A low-contamination method for hydrothermal decomposition of zircon and extraction of U and Pb for isotopic age determinations. Geochim. Cosmochim. Acta 37, 485–494.

Krogh, T., 1982. Improved accuracy of U-Pb zircon ages by the creation of more concordant systems using an air abrasion technique. Geochim. Cosmochim. Acta 46, 637–649.

Lissenberg, C.J., Zagorevski, A., McNicoll, V.J., van Staal, C.R., Whalen, J.B., 2005. Assembly of the Annieopsquotch accretionary tract, Newfoundland Appalachians: Age and geodynamic constraints from syn-kinematic intrusions. J. Geol. 113, 553–570.

Ludwig, K.R., 2003. User's manual for isoplot 3.00, a geochronlogical toolkit for microsoft excel. Berkeley Geochronl. Cent. Spec. Publ. 4, 25–32.

Marocchi, M., Hermann, J., Tropper, P., Bargossi, G.M., Mair, V., 2010. Amphibole and phlogopite in "hybrid" metasomatic bands monitor trace element transfer at the interface between felsic and ultramafic rocks (Eastern Alps, Italy). Lithos 117, 135–148.

Marschall, H.R., Schumacher, J.C., 2012. Arc magmas sourced from mélange diapirs in subduction zones. Nat. Geosci. 5, 862–867.

Marschall, H.R., Altherr, R., Rüpke, L., 2007. Squeezing out the slab—modelling the release of Li, be and B during progressive high-pressure metamorphism. Chem. Geol. 239, 323–335.

Mattinson, J.M., 2005. Zircon U–Pb chemical abrasion ("CA-TIMS") method: combined annealing and multi-step partial dissolution analysis for improved precision and accuracy of zircon ages. Chem. Geol. 220, 47–66.

Nilsen, O., Wolff, F.C., 1989. Røros og Sveg. Berggrunnskart Røros og Sveg M 1:250000. Undersøkelse, Norges Geologiske.

Nilsen, O., Sundvoll, B., Roberts, D., Corfu, F., 2003. U-Pb geochronology and geochemistry of trondhjemites and a norite pluton from the SW Trondheim Region. Central Norwegian Caledonides: Norges Geologiske Undersøkelse Bull. 441, 5–16.

Pearce, J.A., 1996. A user's guide to basalt discrimination diagrams: Trace element geochemistry of volcanic rocks: applications for massive sulphide exploration. Geological Association of Canada, Short Course Notes. 12, pp. 79–113.

Pearce, J.A., 2008. Geochemical fingerprinting of oceanic basalts with applications to ophiolite classification and the search for Archean oceanic crust. Lithos 100, 14–48.

Pearce, J.A., Peate, D.W., 1995. Tectonic implications of the composition of volcanic arc magmas. Annu. Rev. Earth Planet. Sci. 23, 251–285.

Peccerillo, A., 1999. Multiple mantle metasomatism in Central-Southern Italy: geochemical effects, timing and geodynamic implications. Geology 27, 315–318.

Peccerillo, A., Martinotti, G., 2006. The Western Mediterranean lamproitic magmatism: origin and geodynamic significance. Terra Nova 18, 109–117.

Pedersen, R., Bruton, D., Furnes, H., 1992. Ordovician faunas, island arcs and ophiolites in the Scandinavian Caledonides. Terra Nova 4, 217–222.

Pe-Piper, G., Piper, D.J., Koukouvelas, I., Dolansky, L.M., Kokkalas, S., 2009. Postorogenic shoshonitic rocks and their origin by melting underplated basalts: the Miocene of Limnos. Greece. Geol. Soc. Am. Bull. 121, 39–54.

Pérez-Valera, L.A., Rosenbaum, G., Sánchez-Gómez, M., Azor, A., Fernández-Soler, J.M., Pérez-Valera, F., Vasconcelos, P.M., 2013. Age distribution of lamproites along the Socovos Fault (southern Spain) and lithospheric scale tearing. Lithos 180, 252–263.

Plank, T., 2005. Constraints from thorium/lanthanum on sediment recycling at subduction zones and the evolution of the continents. J. Petrol. 46, 921–944.

Plank, T., Langmuir, C.H., 1998. The chemical composition of subducting sediment and its consequences for the crust and mantle. Chem. Geol. 145, 325–394.

Prelević, D., Foley, S., Romer, R., Cvetković, V., Downes, H., 2005. Tertiary ultrapotassic volcanism in Serbia: constraints on petrogenesis and mantle source characteristics. J. Petrol. 46, 1443–1487.

Prelević, D., Foley, S., Romer, R., Conticelli, S., 2008. Mediterranean Tertiary lamproites derived from multiple source components in postcollisional geodynamics. Geochim. Cosmochim. Acta 72, 2125–2156.

Prelević, D., Jacob, D.E., Foley, S.F., 2013. Recycling plus: a new recipe for the formation of Alpine–Himalayan orogenic mantle lithosphere. Earth Planet. Sci. Lett. 362, 187–197.

Qian, Q., Hermann, J., 2013. Partial melting of lower crust at 10–15 kbar: constraints on adakite and TTG formation. Contrib. Mineral. Petrol. 165, 1195–1224.

Roberts, D., Gee, D., 1985. An introduction to the structure of the Scandinavian Caledonides. The Caledonide orogen–Scandinavia and related areas 1, 55–68.

Rudnick, R.L., Gao, S., 2003. Composition of the continental crust. Treatise on geochemistry 3, 659.

Ryan, J.G., 2002. Trace-element systematics of beryllium in terrestrial materials. Rev. Mineral. Geochem. 50, 121–145.

Schmidt, M.W., Vielzeuf, D., Auzanneau, E., 2004. Melting and dissolution of subducting crust at high pressures: the key role of white mica. Earth Planet. Sci. Lett. 228, 65–84.

Schmitz, M.D., Schoene, B., 2007. Derivation of isotope ratios, errors, and error correlations for U-Pb geochronology using 205Pb-235U-(233U)-spiked isotope dilution thermal ionization mass spectrometric data. Geochem. Geophys. Geosyst. 8, 8.

Shafaii Moghadam, H., Griffin, W.L., Kirchenbaur, M., Garbe-Schönberg, D., Zakie Khedr, M., Kimura, J.-I., Stern, R.J., Ghorbani, G., Murphy, R., O'Reilly, S.Y., 2018. Roll-back, extension and mantle upwelling triggered eocene potassic magmatism in NW Iran. J. Petrol. 59, 1417–1465.

Slagstad, T., Kirkland, C.L., 2018. Timing of collision initiation and location of the Scandian orogenic suture in the Scandinavian Caledonides. Terra Nova 30, 179–188.

Slagstad, T., Pin, C., Roberts, D., Kirkland, C.L., Grenne, T., Dunning, G., Sauer, S., Andersen, T., 2014. Tectonomagmatic evolution of the early Ordovician suprasubduction-zone ophiolites of the Trondheim Region, Mid-Norwegian Caledonides. Geol. Soc. Lond. Spec. Publ. 390, 541–561.

Soder, C.G., Romer, R.L., 2018. Post-collisional potassic–ultrapotassic magmatism of the Variscan Orogen: implications for mantle metasomatism during continental subduction. J. Petrol. 59, 1007–1034.

Spandler, C., Pirard, C., 2013. Element recycling from subducting slabs to arc crust: a review. Lithos 170, 208–223.

Spandler, C., Hermann, J., Arculus, R., Mavrogenes, J., 2003. Redistribution of trace elements during prograde metamorphism from lawsonite blueschist to eclogite facies; implications for deep subduction-zone processes. Contrib. Mineral. Petrol. 146, 205–222.

Stacey, J.T., Kramers, J., 1975. Approximation of terrestrial lead isotope evolution by a two-stage model. Earth Planet. Sci. Lett. 26, 207–221.

Stokke, E.W., Gasser, D., Dalslåen, B.H., Grenne, T., 2018. Tectonic evolution of syn-to late-orogenic sedimentary–volcanic basins in the central Norwegian Caledonides. J. Geol. Soc. Lond. 175, 605–618.

Sun, S.-S., McDonough, W.-s., 1989. Chemical and isotopic systematics of oceanic basalts: implications for mantle composition and processes. Geol. Soc. Lond. Spec. Publ. 42, 313–345.

Svensen, H.H., Hammer, Ø., Corfu, F., 2015. Astronomically forced cyclicity in the Upper Ordovician and U–Pb ages of interlayered tephra, Oslo Region, Norway. Palaeogeogr. Palaeoclimatol. Palaeoecol. 418, 150–159.

Thompson, R., Fowler, M., 1986. Subduction-related shoshonitic and ultrapotassic magmatism: a study of Siluro-Ordovician syenites from the Scottish Caledonides. Contrib. Mineral. Petrol. 94, 507–522.

Tommasini, S., Avanzinelli, R., Conticelli, S., 2011. The Th/La and Sm/La conundrum of the Tethyan realm lamproites. Earth Planet. Sci. Lett. 301, 469–478.

Tucker, R.D., Robinson, P., Solli, A., Gee, D.G., Thorsnes, T., Krogh, T.E., Nordgulen, Ø., Bickford, M., 2004. Thrusting and extension in the Scandian hinterland, Norway: New U-Pb ages and tectonostratigraphic evidence. Am. J. Sci. 304, 477–532.

Vogt, T., 1945. The geology of part of the Hølonda-Horg district, a type area in the Trondheim region. Nor. Geol. Tidsskr. 25, 449–528.

West, D.P., Tomascak, P.B., Coish, R.A., Yates, M.G., Reilly, M.J., 2007. Petrogenesis of the ultrapotassic Lincoln Syenite, Maine: late Silurian-early Devonian melting of a source region modified by subduction driven metasomatism. Am. J. Sci. 307, 265–310.

White, J.D., 2000. Subaqueous eruption-fed density currents and their deposits. Precambrian Res. 101, 87–109.